FACULDADE DE ENGENHARIA DA UNIVERSIDADE DO PORTO

Haemorheology and haemodynamics numerical study in right coronary arteries

Ernesto António Morais Romano

MASTER THESIS

Integrated Master in Mechanical Engineering

Supervisor: Prof. Sónia Isabel Silva Pinto

Co-Supervisor: Prof. Catarina Rosa Santos Ferreira de Castro

July 16, 2019

Haemorheology and haemodynamics numerical study in right coronary arteries

Ernesto António Morais Romano

Integrated Master in Mechanical Engineering

July 16, 2019

Abstract

Cardiovascular diseases have their primary cause in blood flow pathologies. Numerical fluid dynamics simulation has proven to be a practical and efficient tool for the modelling of blood flow, allowing a better understanding of cardiovascular diseases, the leading cause of death in developed countries, such as atherosclerotic disease.

Haemodynamic analysis of blood flow requires an accurate characterization of the rheological behaviour of blood by constitutive models relating the stress to the rate of deformation of the flow. The models commonly used are usually simplifications, only considering blood as a Newtonian fluid or a purely shear-thinning non-Newtonian fluid. However, experimental studies have shown that blood flow exhibits other non-Newtonian characteristics such as viscoelasticity. The constant progress in the field of haemorheology, that studies flow and deformation behaviour of blood, is derived from its clinical interest.

The present work aims to study the dynamic behaviour of the blood flow while considering constitutive models for blood that depict its viscoelastic property. For this purpose, different rheological models for blood where implemented in the ANSYS FLUENT commercial software by writing additional code through the use of User-Defined Functions (UDF).

Three different idealized right coronary arteries geometries were used in a comparative numerical study of different Newtonian, purely shear-thinning non-Newtonian and viscoelastic non-Newtonian models. Results for velocity contours and profiles were used in direct comparison to illustrate the influence of the shear-thinning and viscoelastic effects on the behaviour of blood flow. When considering the elastic properties of blood, in particular for the multi-mode viscoelastic constitutive models for blood, there is a significant reduction in axial velocity in the core regions of the flow. Regions with higher velocity gradients, such as bifurcations or stenosed regions, have also shown an increased impact of the viscoelastic effects in the flow. The reduced velocities in the viscoelastic models result in a decrease of the wall shear stress distribution, the peak values being close to half the magnitude (51%) of purely shear-thinning models.

To study the effects of considering the viscoelastic property of blood on the numerical tools for diagnostic and prevention of cardiovascular diseases, more realistic scenarios were also analysed by using patient-specific models of right coronary arteries. Haemodynamic wall shear stress-based descriptors, which indicate the tendency for atherosclerosis development, were determined for two healthy patient-specific cases. The wall shear stress reduction throughout the cardiac cycle, due to the use of a viscoelastic constitutive model, has a noticeable impact on the calculated haemodynamic descriptors. In the studied cases, it led to the appearance of new atherosusceptible regions that would not be found critical if other non-viscoelastic rheological models were used.

The viscoelastic models allow for a more realistic study of patient pathology and, therefore, an improved tool for prevention, diagnosis and treatment of cardiovascular diseases.

Keywords: Haemodynamics, haemorheology, blood, viscoelasticity, computational fluid dynamics, user-defined functions, atherosclerosis, right coronary artery

Resumo

Doenças cardiovasculares têm como causa primária alterações no comportamento do fluxo sanguíneo. A simulação numérica da dinâmica de fluidos mostrou ser uma ferramenta prática e eficiente para a modelação do fluxo do sangue, permitindo um melhor entendimento de doenças cardiovasculares, a principal causa de morte em países desenvolvidos, tal como a doença aterosclerótica.

A análise hemodinâmica do fluxo sanguíneo necessita de uma caracterização precisa do comportamento reológico do sangue por modelos constitutivos que relacionam a tensão com a taxa de deformação do fluxo. Os modelos mais utilizados são geralmente simplificações, apenas considerando o sangue como um fluido Newtoniano ou como um fluido não-Newtoniano puramente pseudoplástico. Contudo, estudos experimentais demonstraram que o fluxo sanguíneo contém outras características não-Newtonianas tal como a viscoelasticidade. O progresso constante no ramo da hemorreologia, estudo do comportamento do fluxo e da deformação do sangue, é derivado do seu interesse clínico.

Este trabalho visa estudar o comportamento dinâmico do fluxo sanguíneo considerando modelos constitutivos para o sangue que retratem a sua propriedade viscoelástica. Para tal, foram implementados diferentes modelos reológicos do sangue no *software* comercial ANSYS FLUENT através da escrita de código adicional, usando *User-Defined Functions* (UDF).

Três geometrias idealizadas de artérias coronárias direitas diferentes foram usadas num estudo comparativo numérico de diferentes modelos Newtonianos, não-Newtonianos puramente pseudoplásticos e não-Newtonianos viscoelásticos. Resultados de mapas e perfis de velocidade foram utilizados em comparação direta para ilustrar a influência dos efeitos pseudoplásticos e viscoelásticos no comportamento do fluxo sanguíneo. Quando se consideram as propriedades elásticas do sangue, em particular, considerando os modelos constitutivos viscoelásticos multi-modo para o sangue, há uma redução significativa da velocidade axial nas regiões centrais do fluxo. Regiões com gradientes de velocidade superiores, tais como bifurcações ou zonas com estenose, demonstraram também um aumento do impacto dos efeitos viscoelásticos no fluxo. As velocidades reduzidas nos modelos viscoelásticos resultam numa diminuição da distribuição de tensão de corte na parede, cujos valores máximos são aproximadamente metade (51%) dos valores considerando os modelos puramente pseudoplásticos.

De modo a estudar os efeitos de considerar a propriedade viscoelástica do sangue nas ferramentas numéricas para prevenção e diagnóstico de doenças cardiovasculares, cenários mais realistas foram também analisados através de geometrias específicas de pacientes de artérias coronárias direitas. Descritores hemodinâmicos baseados na tensão de corte na parede, que indicam a tendência do aparecimento de aterosclerose, foram determinados para dois casos de artérias saudáveis. A redução da tensão de corte na parede ao longo de todo o ciclo cardíaco, devido ao uso de um modelo constitutivo viscoelástico, tem um impacto notável nos descritores hemodinâmicos calculados. Nos casos em estudo, levou ao aparecimento de novas zonas aterosuscetíveis que não seriam consideradas críticas se tivesse sido utilizado outro modelo reológico não viscoelástico.

Os modelos viscoelásticos permitem um estudo mais realista da patologia do paciente e, portanto, uma ferramenta melhorada de prevenção, diagnóstico e tratamento de doenças cardiovasculares.

Palavras-chave: Hemodinâmica, hemorreologia, sangue, viscoelasticidade, dinâmica de fluidos computacional, *user-defined functions*, aterosclerose, artéria coronária direita

Acknowledgements / Agradecimentos

Gostaria de tomar esta oportunidade para agradecer a todas as pessoas que permitiram o sucesso e a elaboração deste trabalho, dada a ajuda que me forneceram, quer de forma direta ou indireta, durante este percurso.

Em primeiro lugar gostaria de agradecer às minhas supervisoras. À Prof. Sónia Pinto, pela orientação e por todo o apoio contínuo que foram essenciais no decorrer deste trabalho. À Prof. Catarina Castro, em particular, pela oportunidade de poder contribuir para este desafiante projeto de engenharia e também por todo o apoio e aconselhamento no desenvolvimento do mesmo.

Agradeço também à Faculdade de Engenharia da Universidade do Porto e a todas as instituições que contribuíram de modo imprescindível para o desenvolvimento deste estudo - o INEGI, o DEMec, a FMUP e ao Centro Hospitalar de Vila Nova de Gaia/ Espinho. O autor gostaria ainda de agradecer os fundos atribuídos pela Fundação para a Ciência e Tecnologia (FCT), Portugal, através do "Associated Laboratory of Energy, Transports and Aeronautics (LAETA)", UID/EMS/50022/2019.

Aos meus pais, por toda uma vida de apoio incondicional, sendo os responsáveis por este culminar do meu percurso académico. Deram-me tudo o que alguma vez poderia sonhar e ainda mais, e só tenho de agradecer por isso e ao mesmo tempo pedir desculpa por ter aproveitado tão pouco.

À minha família e à minha irmã, por todo o carinho e toda a preocupação.

Aos meus amigos, em particular os que comigo fizeram lado a lado este percurso, um obrigado especial. Foi difícil, mas para mim certamente não o foi tanto, dado que não tinha o problema de ter de me ouvir falar sobre fluidos.

Por fim, queria agradecer à minha namorada Joana: foste a razão para eu vir todos os dias trabalhar com um sorriso e sem qualquer remorso. Por todos os encontros para café pelas manhãs e por todo o amor, motivação e paciência em qualquer momento.

Ernesto Romano

"Don't give yourselves to these unnatural men
- machine men with machine minds and machine hearts!
You are not machines! You are not cattle! You are men!"

Sir Charles Spencer Chaplin

Contents

List of Figures

List of Tables

Symbols and Abbreviations

Abbreviations

Ao	Aorta
AV	Aortic valve
CAD	Coronary artery disease
CFD	Computational fluid dynamics
CT	Computed tomography
FSI	Fluid-structure interaction
GNM	Generalized Newtonian model
GOB	Generalized Oldroyd-B
IVC	Inferior vena cava
LA	Left atrium
LV	Left ventricle
MV	Mitral valve
NS	Newtonian model
PA	Pulmonary artery
PDE	Partial differential equation
PTT	Phan-Thien/ Tanner
PV	Pulmonary vein
PVv	Pulmonary valve
RA	Right atrium
RBC	Red blood cell
RCA	Right coronary artery
RV	Right ventricle
sPTT	Simplified Phan-Thien/ Tanner
SVC	Superior vena cava
TV	Tricuspid valve
UDF	User-defined function
UDS	User-defined scalar
WBC	White blood cell
WSS	Wall shear stress

Symbols

$\triangledown$	Upper-convected derivative
$\square$	Gordon-Schowalter convected derivative
D	Diameter $[m]$
$\mathbf{D}$	Strain rate tensor $[s^{-1}]$
$\mathbf{e}_n$	Unit normal vector
G	Young's modulus $[MPa]$
$I_{\mathbf{D}}$	First principal invariant of the strain rate tensor $[s^{-1}]$
$II_{\mathbf{D}}$	Second principal invariant of the strain rate tensor $[s^{-1}]$
$III_{\mathbf{D}}$	Third principal invariant of the strain rate tensor $[s^{-1}]$
$\mathbf{I}$	Identity matrix
i	Imaginary unit
J_o	First order Bessel function
L	Length $[m]$
N_1	First normal stress difference $[Pa]$
N_2	Second normal stress difference $[Pa]$
n	Characteristic constant of the flow
OSI	Oscillatory Shear Index
p	Pressure $[Pa]$
Q	Flow rate $[m^3/s]$
R	Radius $[m]$
Re	Reynolds number
RRT	Relative Residence Time $[Pa^{-1}]$
r	Radial distance from the axis $[m]$
S	Source term
s	Location
T	Cardiac cycle duration $[s]$
$\mathbf{T}$	Cauchy stress tensor $[Pa]$
$TAWSS$	Time Averaged Wall Shear Stress $[Pa]$
t	Time $[s]$
$\mathbf{t}$	Wall traction $[Pa]$
U	Mean velocity $[m/s]$
$\mathbf{u}$	Velocity vector $[m/s]$
W_o	Womersley number
$\mathbf{WSS}$	Wall Shear Stress vector $[Pa]$

Greek Symbols

α	Mobility factor
$\dot{\gamma}$	Shear rate $[s^{-1}]$
ε	Extensibility coefficient
λ	Relaxation time $[s]$
μ	Dynamic viscosity $[Pa \cdot s]$
μ_e	Elastic viscosity $[Pa \cdot s]$
μ_f	Blood viscosity $[Pa \cdot s]$
μ_s	Solvent viscosity $[Pa \cdot s]$
μ_0	Zero shear viscosity $[Pa \cdot s]$
μ_∞	Infinite shear viscosity $[Pa \cdot s]$
ρ	Density $[kg/m^3]$
ρ_f	Blood density $[kg/m^3]$
$\boldsymbol{\tau}$	Extra stress tensor $[Pa]$
$\boldsymbol{\tau}_e$	Elastic contribution of the extra stress tensor $[Pa]$
$\boldsymbol{\tau}_s$	Solvent contribution of the extra stress tensor $[Pa]$
ω	Angular frequency $[rad/s]$
ω_f	Cardiac frequency $[rad/s]$

Chapter 1

Introduction

Cardiovascular diseases are the leading cause of death in developed countries [1]. In particular, about 7 million people die annually due to coronary heart disease [2, 3]. Atherosclerosis is the outcome of the progressive accumulation of lipids on the arterial walls leading to a narrowing of the blood vessel. The resultant stenosis formed by the atherosclerotic plaque can lead to alterations in the haemodynamic behaviour of blood, such as increased flow velocities, high shear stress and flow recirculation [4]. When the wall shear stress increases in the narrowed vessel, a rupture may occur.

Computational fluid dynamics (CFD) has proven to be a practical and efficient tool for the modelling of blood flow, allowing a better understanding of cardiovascular diseases [5, 6]. However, the performance of CFD models is directly dependent on the accuracy of the model. Uncertainties in the solutions are sometimes due to limited computational resources or due to strong simplifications of the physiological conditions. As such, for numerical fluid dynamics simulation to be used as a tool for diagnostic and treatment of cardiovascular diseases, a good understanding of haemodynamics, blood rheology and physiological flow conditions is needed.

When looking into the matter of blood rheology, or haemorheology, a considerable amount of viscosity models can be found, although none of them has been agreed upon [5]. Blood exhibits non-Newtonian behaviour which is further emphasized due to the pulsatile nature of blood flow and the small-scale lengths in question. Different levels of simplification have been considered when describing blood rheology. Although the rheological behaviour of human blood can be considered Newtonian for high enough shear rates, in small vessels the elastic effects should not be neglected [6].

The present work focuses on the complex rheological nature of blood, focusing on the modelling blood as a viscoelastic non-Newtonian fluid, in order to obtain a more reliable and realistic tool for the prevention and diagnosis of atherosclerotic disease.

1.1 Objectives

The necessity for better CFD tools able to describe increasingly realistic models of blood flow has already been introduced. Despite the existence of several in-house codes, the advantages and commodities provided by commercial software are of great importance in supporting the generalization of the diagnostic tools in question. As such, the main objective of this thesis can be described through the following key points:

- Investigate the non-Newtonian properties of blood, focusing in particular on the different existing viscoelastic constitutive models;
- Perform numerical simulations of blood flow in ANSYS Fluent, a user-friendly commercial solver widely used by many authors, while considering these more realistic rheological models, implemented through User-Defined-Functions;
- Study the effects of considering the viscoelastic property of blood in the velocity and wall shear stress distributions, and the resulting haemodynamic descriptors which indicate the tendency for atherosclerosis appearance in patient-specific right coronary arteries.

1.2 Structure of the dissertation

The present thesis is organized as follows: Chapter 2 provides an introduction to the anatomy and physiology of the cardiovascular system, as well as to the atherosclerotic disease; Chapter 3 focuses on haemodynamics and blood flow, providing all the fluid mechanics concepts which are dealt with throughout the dissertation; In Chapter 4 the different aspects of blood rheology and of the mechanical properties of blood are introduced, along with a discussion of some different viscoelastic constitutive models; In Chapter 5 the methodology applied in all numerical simulations is exposed, while introducing the workings behind the User-Defined Functions of ANSYS Fluent and their usage to implement rheological models not present in the software; In Chapter 6 results for the velocity and wall shear stress distributions of the implemented rheological models are presented and discussed for both idealized and patient-specific geometries; Finally, Chapter 7 includes a summary of the present work as well as the conclusions of this thesis, along with some suggestions for future work.

Chapter 2

Cardiovascular system

A basic understanding of the anatomy and physiology of the cardiovascular system is needed to achieve the objective of cardiovascular modelling. In this chapter a very brief introduction to the subject will be made, focusing in the mechanical properties of the system and the aspects which will be discussed in following chapters.

The cardiovascular system is composed by the heart, which acts as pump and is responsible for the circulation of blood, and a closed network of blood vessels that convey blood to the body (arteries), afterwards draining it to the heart (veins). Figure 2.1 shows a simplified representation of this system. The cardiovascular system contributes to homeostasis of other body systems by transporting and distributing blood throughout the body to deliver materials (such as oxygen, nutrients, and hormones) and carrying away wastes [2, 7].

2.1 Heart

The heart is a muscular organ made almost entirely of myocardium. It has four cavities: the upper left (LA) and right (RA) atria, and the lower left (LV) and right (RV) ventricles, responsible for the main contraction and propelling of blood into the arteries. The upper cavities, the atria, are connected to the lower ones, the ventricles, through the tricuspid valve (TV) on the right side and the mitral valve (MV) on the left side . The heart is composed by two synchronized parallel pumps. The one on the right collects deoxygenated blood in right atrium, from the systemic veins superior (SVC) and inferior (IVC) vena cava, passes to the RV and perfuses the lungs through the pulmonary valve (PVv) into the main pulmonary artery (PA). The left side collects oxygenated blood from the pulmonary veins (PV) into the left atrium, passes through the MV to the LV and perfuses the rest of the body through the aortic valve (AV) and into the aorta (Ao) (Figure 2.2) [1].

2.1.1 Cardiac cycle

The heart beat is a two stage pumping action with a duration of approximately one second. The systole is the period when the heart cavities contract and blood is ejected. The opposing period

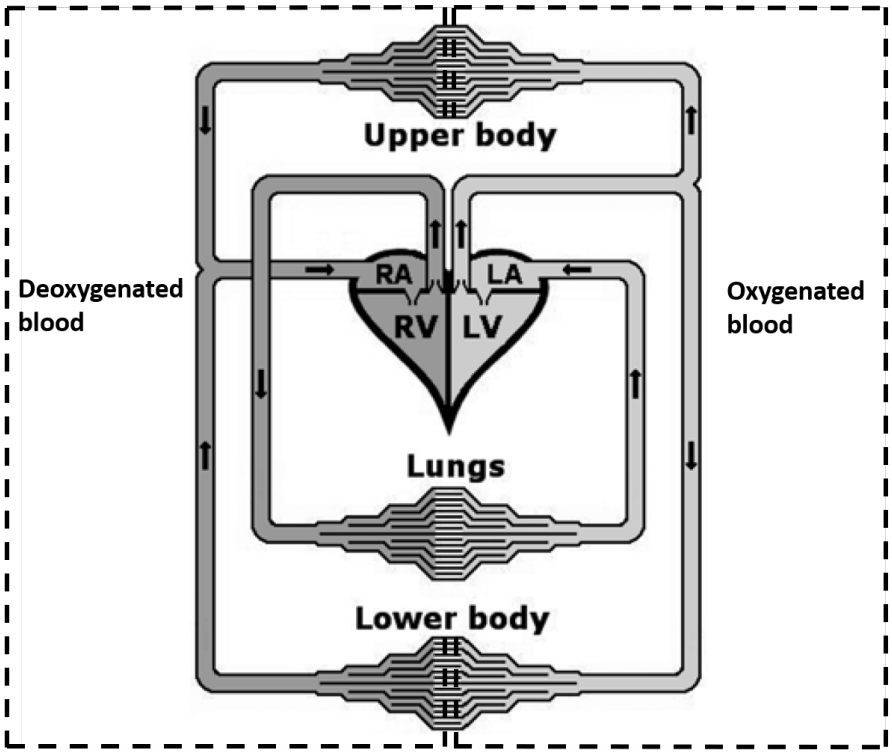

Figure 2.1: Schematics of the cardiovascular system. Adapted from [1].

is the diastole, when there is a relaxation of the myocardium and the heart fills with blood. The diastole occupies approximately two thirds of the cardiac cycle.

When the ventricular systole begins, the pressure in the ventricles increases rapidly, exceeding the pressure in the atria and causing the connecting valves to close. As all the valves are closed and blood is incompressible this will enable an even faster increase in pressure, forcing the aortic valve (or the pulmonary valve in the case of the right side of the heart) to open and the blood to be expelled. After a short time the myocardium begins to relax and the pressure difference between the left ventricle (LV) and the aorta (Ao), and the right ventricle (RV) and the pulmonary artery (PA), reverses, becoming positive. This positive pressure gradient decelerates the flow, which eventually starts to reverse. To stop this flow reversal the AV and PVv valves close. When the diastole is over and the pressure in the ventricles is lower than in the atria, the MV and TV open, beginning the ventricular filling [2, 1].

2.2 Vascular networks

There are five main types of blood vessels: arteries, arterioles, capillaries, venules and veins. As already mentioned, the primary purpose of the arterial and venous vessels is to carry blood to and from the various tissues. Arteries carry blood away from the heart to other organs. These branch and divide into even smaller arteries called arterioles. Upon entering contact with a tissue, arterioles branch into multiple vessels called capillaries. These reunite to form venules which then

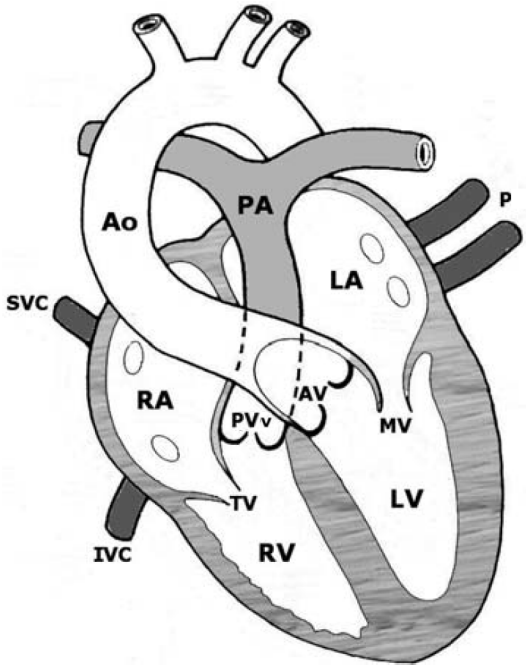

Figure 2.2: Schematics of the gross anatomy of a cross section of the heart. Adapted from [1].

progressively enlarge to form veins. Veins are vessels that convey blood from the tissues back to the heart [7].

2.2.1 Right Coronary Artery

Due to the multiple layers that make up the heart walls, nutrients from the blood within its cavities are not able to diffuse fast enough to supply the heart. For this reason, the myocardium has its own set of blood vessels known as coronary circulation. There are two coronary arteries, left and right, that branch from the ascending aorta and encircle the heart (Figure 2.3), transporting oxygenated blood during the relaxation of the myocardium. The right coronary artery (RCA) supplies small branches to the right atrium, ultimately diving into the posterior ventricular and marginal branches [2].

2.3 Atherosclerosis

There are several types of cardiovascular diseases, such as heart failures, genetic disorders or diseases due to the blockage of blood vessels. Blockages in the heart are commonly called heart attacks, while blockages in the brain are called strokes. Together they compromise almost half of all deaths, making cardiovascular diseases the leading cause of death in developed countries [1]. In particular, coronary artery disease (CAD) affects about 7 million people annually. CAD results from the accumulation of atherosclerotic plaques in coronary arteries, leading to a reduction in blood flow to the heart [2]. Atherosclerosis is the progressive formation of plaques on the arterial

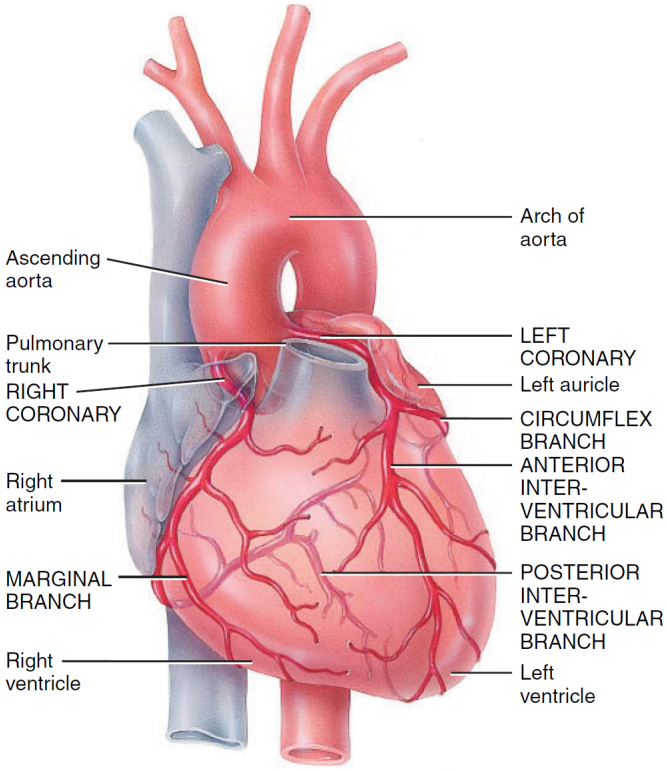

Figure 2.3: Anterior view of coronary arteries [2].

walls due to the accumulation of fatty material, fibrous elements and calcium (Figure 2.4). This is a progressive disease that can take decades until the appearance of any symptoms, such as chest pain or even heart attack and blood vessel ruptures, due to the obstruction of the stenosis. Although atherosclerosis can also occur in arteries outside the heart, it is more common in coronary arteries and it is close to unknown in pulmonary arteries or in the venous system. This apparent behaviour could be explained by the strong focal nature of this lesion, which is commonly found in bends in tortuous arteries and on the outer walls of bifurcations.

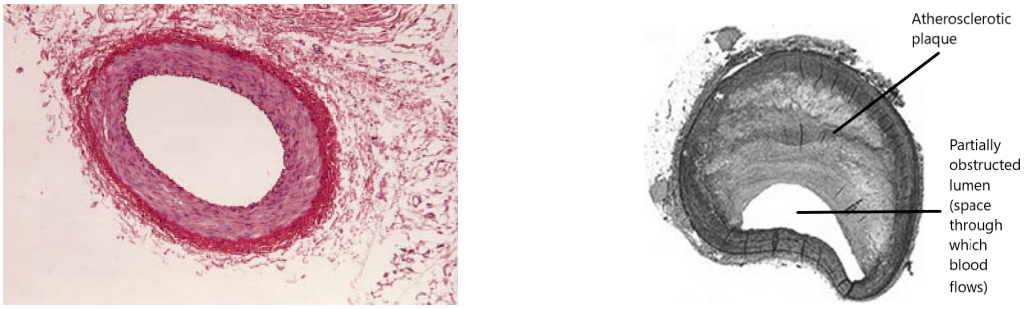

(a) (b)

Figure 2.4: Transverse section of a normal artery (a) and one partially obstructed by an atherosclerotic plaque (b). Adapted from [2, 1].

Chapter 3

Haemodynamics

Haemodynamics is the study of blood flow in the cardiovascular system discussed in Chapter 2. The circulatory system is composed by a pump - the heart - and multiple branching tubes (the blood vessels) where blood flows [8]. The arterial blood flow in the human body is typically a multiphase non-Newtonian pulsatile flow. In order to gain further insight into this system and the dependencies of blood flow, it is helpful to start by introducing some notions in the mechanics of fluid flow.

3.1 Fluid mechanics and blood flow

Flow can be characterized as either steady or unsteady. A flow can be said to be steady if the flow velocity is constant in time at every location [9]. Blood flow shows, however, a high degree of unsteadiness due to its pulsatile nature.

Another way to describe fluid flow is by introducing the notion of laminar or turbulent flows. This distinction is usually done by association of a dimensionless parameter, the Reynolds number, that physically represents the ratio of inertial forces to viscous forces. If a pipe of characteristic diameter D is considered, the Reynolds number, Re_D, for an internal flow of mean velocity U is given by:

$$Re_D = \frac{\rho U D}{\mu} \tag{3.1}$$

where μ is the dynamic viscosity of the Newtonian fluid and ρ its density. The suffix D indicates that the reference length in use is the diameter but this could be changed in different geometries for another characteristic length. In laminar flow the fluid motion is smooth and ordered, while in turbulent flows there are unpredictable variations in velocity. If the flow in a pipe is still considered, it is only the fluid velocity that will determine the character of the flow, as the characteristic length is unchanged and the fluid properties are considered constant. For laminar flow in a pipe there will only be a single velocity component, along the axis, and although the flow

may be unsteady this time variation will be predictable. For turbulent flows, the main component for velocity will still be along the pipe but it will be accompanied by random components normal to the pipe axis that represent the unpredictable small disturbances to the velocity field [9, 8]. With large Reynolds numbers, the inertial forces become dominant over viscous forces and the transition from laminar to turbulent flow will occur.

In uniform large arteries, the Reynolds number is high but usually within the laminar range. However, as the Reynolds number is highly dependent of geometry, turbulence may still occur in large enough arteries, stenosed regions, bifurcations and narrow openings [8].

3.1.1 Steady Laminar Flow in a Uniform tube

One of the first studies trying to relate blood flow rate to the imposed pressure gradient is due to J.L.M. Poiseuille [10]. By considering a circular tube of diameter D and length L with a driving pressure ΔP, the flow rate Q can be given by the following relationship known as Poiseuille's law:

$$Q = \frac{\pi}{128}\frac{\Delta P D^4}{L\mu} \tag{3.2}$$

The relationship in Equation (3.2) is only true when the tube is rigid and of constant cross section, the fluid is Newtonian and under a steady laminar flow, not subject to any entrance effects (disturbances associated to the entrance of the fluid in the tube).

3.1.2 Governing Equations for the motion of fluids

The governing equations that describe the motion of fluids are used in differential analysis of infinitesimal control volumes and are rather complicated non-linear partial differential equations with no exact solution except in some particular cases [9].

In a complete analysis of fluid motion, there is a need to establish a relationship between the stresses acting upon the fluid and velocities. For incompressible Newtonian fluids, i.e., Newtonian fluids with a constant density ρ even when under compression, the normal stresses are given by the Cauchy stress tensor $\mathbf{T}$ and can be expressed as:

$$\mathbf{T} = -p\mathbf{I} + \boldsymbol{\tau} \tag{3.3}$$

where $\boldsymbol{\tau}$ is the extra stress tensor associated with the viscosity of the fluid, $\mathbf{I}$ is the identity matrix and p is the pressure, an isotropic force that acts equally in every direction and is always normal to a surface. The pressure portion of the tensor $\mathbf{I}$ can be written as:

$$\begin{bmatrix} \textit{pressure} \\ \textit{contribution} \\ \textit{to } \boldsymbol{I} \end{bmatrix} = -\begin{bmatrix} p & 0 & 0 \\ 0 & p & 0 \\ 0 & 0 & p \end{bmatrix} = -p\mathbf{I} \tag{3.4}$$

When the fluid is at rest, **T** becomes -p **I**, the hydrostatic pressure [9, 11].

Newtonian fluids follow Newton's law of viscosity. This law states that the extra stress tensor $\boldsymbol{\tau}$ is proportional to the symmetric part of the velocity gradient, **D**:

$$\boldsymbol{\tau} = 2\mu\mathbf{D} \tag{3.5}$$

$$\mathbf{D} = \frac{1}{2}(\nabla\mathbf{u} + \nabla\mathbf{u}^T) \tag{3.6}$$

D is also known as strain rate tensor, and μ is the already introduced dynamic viscosity of the fluid [9].

Taking into account the principles of conservation of mass and conservation of linear momentum for an incompressible fluid and by using the definition of $\boldsymbol{\tau}$ given in Equation (3.3), the governing equations used in flow dynamics can be expressed as:

$$\nabla \cdot \mathbf{u} = 0 \tag{3.7}$$

$$\rho\left(\frac{\partial\mathbf{u}}{\partial t} + \mathbf{u}\cdot\nabla\mathbf{u}\right) = -\nabla p + \nabla\cdot\boldsymbol{\tau} \tag{3.8}$$

where $\boldsymbol{u}$ is the velocity vector. These are the well known incompressible Navier-Stokes Equations that form a system of four partial differential equations (PDEs) that must be solved for the unknown variables p and $\boldsymbol{u}$ with proper initial conditions and boundary conditions. Solving this set of equations represents one of the most common flow modelling techniques known as Computational Fluid Dynamics. These governing equations can also describe fluids with non-Newtonian behaviour. This can be done by using a different constitutive equation or rheological model to describe $\boldsymbol{\tau}$, such as the ones further introduced in Section 4.3.2.

The derivations of the continuity equations and of the equation of motion, Equations (3.7) and (3.8), as well as the principles of conservation of mass and conservation of linear momentum can be found in common fluid mechanics text books [9].

3.1.3 Normal stress differences

When dealing with incompressible non-Newtonian fluids such as blood, it is not possible to achieve separate measurements for the different stress components T_{ii}, τ_{ii} and for the pressure p. This is because the density of an incompressible fluid is (almost) not affected by pressure. If the pressure part of T_{ii} was sought for such a fluid, there would be a need for an independent and accurate measurement of density.

The problem of this separation is not encountered in Newtonian fluids as the normal components τ_{xx}, τ_{yy} and τ_{zz} are zero. However when considering non-Newtonian fluids, without the ability to obtain an independent measurement of p it is not possible to obtain all the components of $\boldsymbol{\tau}$ [11, 12].

Rheologists found a way around this problem by considering normal stress differences instead of normal stresses [11].

$$N_1 \equiv T_{xx} - T_{yy} = \tau_{xx} - \tau_{yy} \tag{3.9}$$

$$N_2 \equiv T_{yy} - T_{zz} = \tau_{yy} - \tau_{zz} \tag{3.10}$$

where N_1 and N_2 are the two independent quantities known as *first* and *second normal stress differences*, formed by the three normal stress components.

3.1.4 Oscillatory flow and Womersley number

As already discussed, blood flow has an unsteady nature, due to the pulsatile pumping action of the heart [8]. The velocity waveforms generated by the heart are complex but can be reproduced by considering a periodic flow of sinusoidal form and frequency ω (the cardiac frequency). This is usually done by the use of the Womersley number, Wo, a non-dimensional flow parameter defined as:

$$Wo = R\sqrt{\frac{\rho\omega}{\mu}} \tag{3.11}$$

where R is the pipe radius. Values for the Womersley number close to 1 are associated to nearly parabolic velocity profiles, while for higher values of Wo the velocity profiles are blunted in the middle, as seen in Figure 3.1.

If an harmonic pressure gradient is considered, given by $\frac{\partial P}{\partial x} = Ae^{i\omega t}$, as a function of time t, then the fully developed velocity profile is:

$$u(r,t) = \frac{AR^2}{i\mu Wo^2}\left(1 - \frac{Jo\left(i^{3/2}Wo\frac{r}{R}\right)}{Jo\left(i^{3/2}Wo\right)}\right)e^{i\omega t} \tag{3.12}$$

where r is the radial distance from the axis, i indicates the imaginary unit and Jo the first order Bessel function [8, 13, 3].

3.1.5 Wall shear stress

Wall shear stress (WSS) is defined as the tangential component of the surface force at the vessel wall, acting against the fluid flow [14, 15]. The traction can be calculated at the wall as $\mathbf{t} = \mathbf{T} \cdot \mathbf{e}_n$ if both the stress tensor $\mathbf{T}$ and the unit normal vector $\mathbf{e}_n$ are taken at a point on the wall surface. The **WSS** vector can then be defined as the tangential component of this wall traction as:

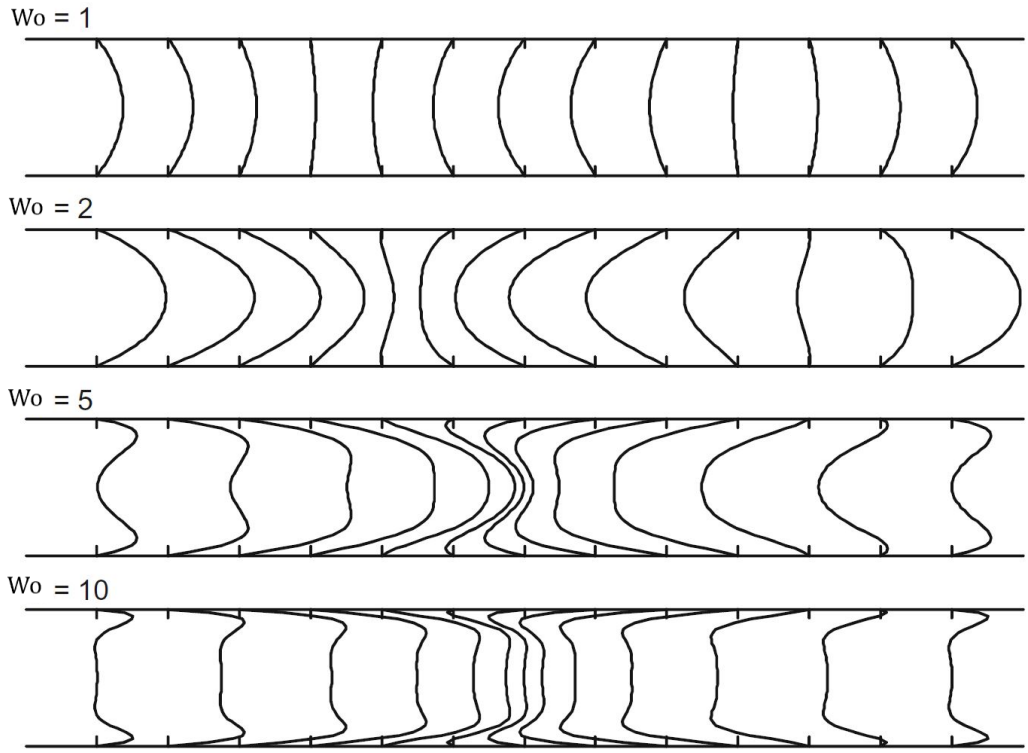

Figure 3.1: Sequences of velocity profiles in a tube with a sinusoidally varying pressure gradient, for indicated values of Womersley number. Adapted from [8].

$$\mathbf{WSS} = \mathbf{t} - (\mathbf{t} \cdot \mathbf{e}_n)\mathbf{e}_n \tag{3.13}$$

3.2 Haemodynamic descriptors

Haemodynamic descriptors are parameters used to summarize haemodynamic behaviour. Most of these descriptors are WSS-based, as WSS is one of the most used parameters in the description of blood flow. Its correlation to cardiovascular diseases is done through the analysis of its temporal and spacial variations during the cardiac cycle [15, 3]. Numerical studies that use this type of descriptors have been a powerful auxiliary tool for the prevention and treatment for atherosclerosis disease.

The first haemodynamic descriptor to be mentioned is the *TAWSS - Time Averaged Wall Shear Stress*, which evaluates the mean value of the WSS magnitude $\left(WSS = \sqrt{WSS_x^2 + WSS_y^2 + WSS_z^2}\right)$ along the cardiac cycle through the following expression:

$$TAWSS(s) = \frac{1}{T}\int_0^T |WSS(s,t)|\ dt \tag{3.14}$$

where T is the cardiac cycle duration and s refers to the location. Lower values for *TAWSS*, below $0.4[Pa]$, indicate a higher probability of plaque formation [3].

OSI - Oscillatory Shear Index is a dimensionless parameter that describes the disturbed flow near surfaces by taking into account the spatial variation of WSS over the cardiac cycle. This haemodynamic descriptor ranges from 0 (no oscillation, **WSS** is unidirectional) to 0.5 (highly disturbed flow with 180º deflections) [3].

$$OSI(s) = 0.5 \left[1 - \frac{\left| \int_0^T \mathbf{WSS}(s,t)\ dt \right|}{\int_0^T |WSS(s,t)|\ dt} \right] \tag{3.15}$$

Lastly the *RRT - Relative Residence Time* descriptor indicates the residence time of particles near the arterial wall. This haemodynamic descriptor is directly depent on the *OSI* and inversely dependent on the *TAWSS*, making it that wall regions with low values for WSS and with high variation of WSS direction (high values of *OSI*) are susceptible to atherosclerosis. RRT values over the threshold of $8[Pa^{-1}]$ indicate zones of risk. This parameter is considered to be the strongest metric of assessing blood flow disruptions [16]:

$$RRT(s) = \frac{1}{(1 - 2 \times OSI) \times TAWSS} \tag{3.16}$$

The considerable variations in both space and time of WSS at any given location, specially when taking into account the complicated geometries of blood vessels and diseased arteries, makes the interpretation of this parameter extremely difficult. Thus, the application and study of haemodynamic descriptors such as the ones presented is of major importance in the field of patient-specific computational fluid dynamics.

Chapter 4

Blood rheology

A possible distinction between fluids and solids is based on their behaviour when under external loads. Fluids can be defined as a substance that continuously deforms (flows) when acted on by a shearing stress, as opposed to common solids [9].

Rheology deals with the flow of complex fluids, through the study of the deformation and flow of matter [11], while its objective consists in determining the flow that would be produced due to applied forces [17].If the fluid in question is blood, the field of investigation is haemorheology.

Most fluids show a behaviour as the one previously described in Chapter 3, where the shearing stress is proportional to the shear rate by a constant called viscosity or dynamic viscosity, at a fixed temperature and pressure. This model for fluid flow is also known as Newton's law of viscosity. The shearing stress is the force per unit area acting parallel to the surface and the shear rate, or rate of shearing strain, is the rate of deformation of the fluid translated into its velocity gradient. This type of fluid is usually designated as Newtonian fluid [9].

However, blood falls under a different category, the non-Newtonian fluids, due to its viscosity being shear rate dependent [5]. Blood can be considered a multiphase, solid-liquid suspension of particles (blood cells, the solid-like phase) suspended in plasma (the liquid phase). Despite plasma showing Newtonian behaviour, blood still has non-Newtonian properties, this being related to its composition, and should only be modelled has a Newtonian fluid in larger vessels [18].

In addition to what is described in Chapter 3 about haemodynamics, blood flow in arteries can be approximately described as a multiphase non-Newtonian pulsatile flow through an elastic tube with small branches. The unsteady nature of blood flow gives way to the necessity of further studying its time-dependent properties, such as viscoelasticity and thixotropy [5].

4.1 Blood composition

Blood is a suspension of a heterogeneous mixture of cells in an aqueous polymer solution, the plasma, which represents approximately 55% of the blood volume. Plasma is composed of 93% water, with the remaining being organic molecules, proteins and ions. The cellular elements of

blood are the red blood cells (RBCs or erythrocytes), white blood cells (WBCs or leukocytes) and platelets (thrombocytes).

Erythrocytes represent 97 to 99% of the cell volume, and the red blood cell fraction of human blood is called haematocrit. RBCs have a biconcave discoid shape with a mean diameter of 8 $[\mu m]$ and are 2 $[\mu m]$ thick. Erythrocytes have an average life span of 3 months and are continuously produced by the bone marrow. The haemoglobin, a protein that is part of its constitution and has a high affinity to oxygen, makes the main function of erythrocytes the transportation of oxygen and carbon dioxide. The high concentration of RBCs will be the main factor in blood rheological properties due to cell deformation and aggregation, and it will be further analysed in the following section [19, 1].

Leukocytes are globular in shape and as cells they are primarily involved in protecting the body against infections, having a life span of only a few days. Despite being much larger than erythrocytes they are less numbered, thus having small effect in the viscosity of blood. However, they are still determinant in flow in micro-circulation [8]. Platelets are non-nucleated cells, discoid in shape that are involved in blood coagulation [19].

4.2 Mechanical Properties of Blood

The mechanical properties of blood are highly dependable on its composition and the respective properties of each component. The presence of these cellular elements and their interactions can cause significant changes to the rheological characteristics of blood [19].

4.2.1 Viscosity

Normal human blood exhibits non-Newtonian shear-thinning behaviour [18]. This type of fluid is characterized by an apparent viscosity that decreases with increasing shear rate. At both ends of the spectrum the apparent viscosity approaches Newtonian behaviour. At low shear rates its value tends to the zero shear viscosity, μ_0, while at high shear rates there is another plateau, the infinite shear viscosity, μ_∞ [17].

Most structured fluids that contain irregularly shaped particles, show a different behaviour at rest and under shear. At rest the particles are oriented randomly in their minimum energy states. When under low levels of shearing these particles resist deformation, granting the fluid a high value of viscosity and in some cases a yield stress. As the shear rate increases the structural units can either disintegrate forming their initial aggregate or align with the direction of the flow and deform along the streamlines, thus leading to the reduction of the apparent viscosity [17]. Figure 4.1 shows a schematic representation of these various micro-structures.

The rheological behaviour of blood can also be described in this way. It has a higher viscosity than plasma, this difference being even more denoted at low shear rates and when the haematocrit rises. At low shear rates the apparent viscosity is high, and it decreases with increasing deformation, approaching a minimum value under high shear forces, as shown in Figure 4.2.

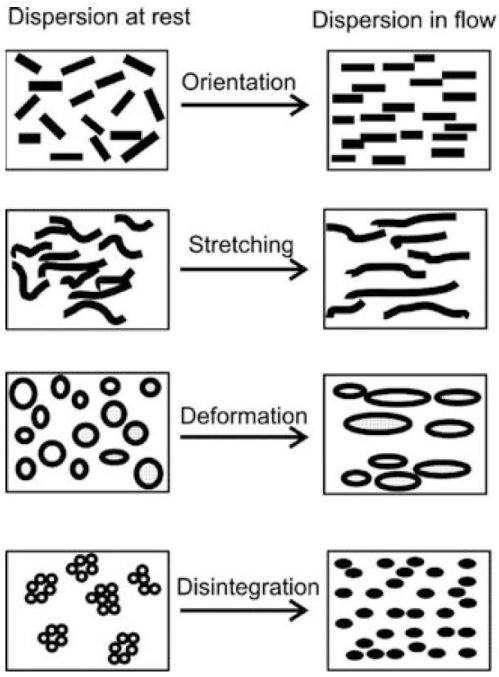

Figure 4.1: Schematics of structures in non-Newtonian dispersions at rest and under shear [17].

This is due to RBC in plasma undergoing reversible aggregation (the rouleaux) which then align with each other interacting to form three-dimensional structures [18, 8]. At low shear rates, this tendency of RBC is responsible for higher viscosity values, due to the disturbance of the flow streamlines. With increasing shear forces, these aggregates become progressively dispersed in the plasma suspension. At higher shear rates, above 400 $[s^{-1}]$, RCBs begin deforming while aligning with the flow and forming layers, losing their biconcave shape and becoming fully elongated [19]. The effect of haematocrit on blood viscosity can be seen in Figure 4.3.

In addition, it is important to note that the formation of rouleaux depends highly on the solution in which the RBCs are suspended. There are solutions other than plasma that can induce this RBC aggregation. However, this has been one of the main setbacks in the measurement of the rheological properties of blood [18], alongside other properties, such as coagulation of blood when in contact with air, that can lead to difficulties in the measuring of viscosity [8].

Blood viscosity is also strongly dependent on temperature [19]. The effects can be significant and as rheological evaluations are usually done under a "room temperature" of 20 to 25 [ºC] as opposed to the normal body temperature of 37 [ºC], care must be taken when comparing results [8].

4.2.2 Viscoelasticity

For an ideal elastic solid, stress is directly proportional to strain, with the constant of proportionality being the material's Young's modulus, G. A viscous fluid is considered to be elastic when

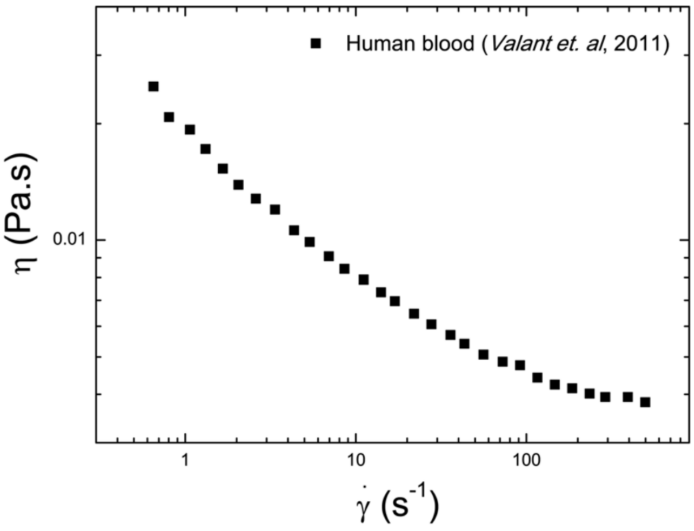

Figure 4.2: Average steady shear viscosity (η) of whole blood measured experimentally by Valant et al. [20].

it has the ability to store and release shear energy. In such fluids with both viscous and elastic properties, a part of the stress is due to strain and another part due to the strain rate [17]. The difference between these components is schematically represented in Figure 4.4. This will be further discussed when looking into the constitutive models for blood, since there will be a need to model viscoelasticity.

In the case of blood, its viscoelastic properties are primarily dependent on the elastic behaviour of erythrocytes [21]. The maximum theoretical value of RBC volume concentration without any deformation is 58%. This means that at normal haematocrit there is little space available for flow to occur without any cell deformation. In fact, blood flow can only happen because RBCs are deformable and can slide in low viscosity plasma layers (Figure 4.5) [8, 21].

All these effects are also further increased due to the pulsatile nature of the flow as well as the elastic properties of the blood vessels. Another important characteristic of the viscoelasticity of blood is the dependence of the elastic stresses on strain. There is a maximum elastic shear stress near unit strain, followed by a decrease in the ability to store elastic energy. This decrease is justified by the dissipation of cell aggregates with increasing shear rates [21].

4.2.3 Thixotropy

There is a large number of definitions for thixotropy. When the subject of study is blood, this property is usually referred to as the dependence of material properties on the time over which shear has been applied [19]. The finite time for the microstructural changes in blood - formation and dissolution of erythrocyte aggregates - is the reason for blood thixotropy. These flow-induced structural changes require less time at higher shear rates than at lower shear rates [21, 8].

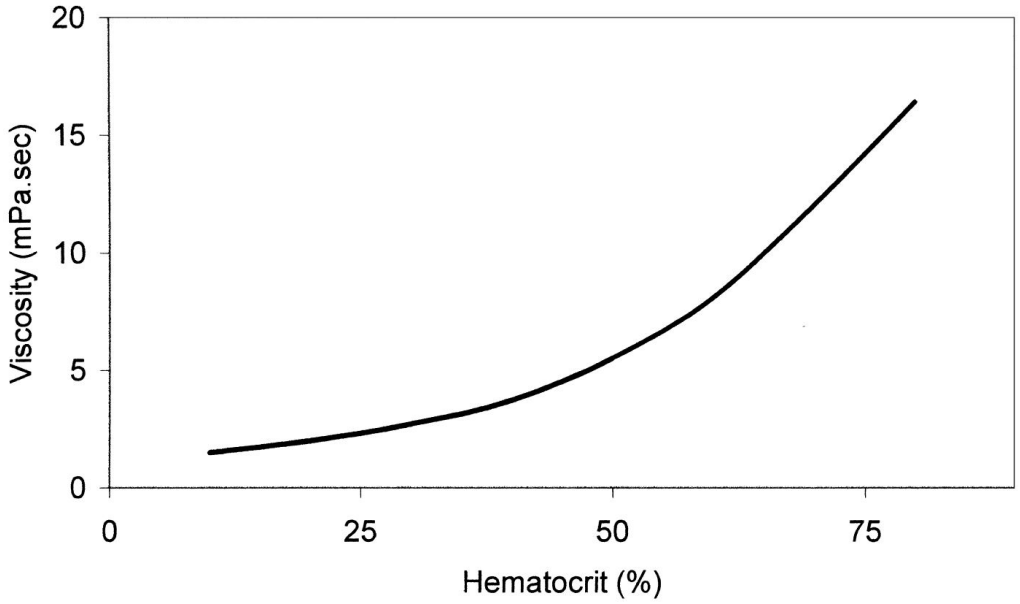

Figure 4.3: Dependence of blood viscosity on haematocrit [18].

It is important to note that although there are constitutive models including this property of blood, most only try to recreate its shear thinning and/or viscoelastic behaviour.

4.2.4 Yield Stress

Yield stress is a threshold above which a material will start to flow. This is considered a non-Newtonian effect as Newtonian fluids always flow when stress is applied [11]. This critical stress level is typically treated as a material property (constant) of the fluid. However, the different experimental methodologies used, the definition of yield stress and the duration of the experiments, give way to fluids having a large range of values for this property. The controversy generated due to the reasons above stated has led researchers to question the pertinence of classifying yield stress as a material property. It was later proposed that yield stress should be treated as a function of time, linked to thixotropy [22].

The reversible formation of rouleaux observed in normal blood is responsible for the existence of yield shear stress. This property, as expected and like the other main rheological properties of blood, is highly haematocrit dependent [8]. This dependence is well represented in Figure 4.6.

4.3 Constitutive models for blood

Rheological constitutive equations are laws of flow that define the value of the extra stress tensor $\boldsymbol{\tau}$ [23, 24]. As already discussed, in large enough vessels, blood shows Newtonian behaviour. Following Newton's law of viscosity introduced in Section 3.1 this tensor is such that it is proportional to the symmetric part of the velocity gradient $\mathbf{D}$, also known as strain rate tensor, as described in

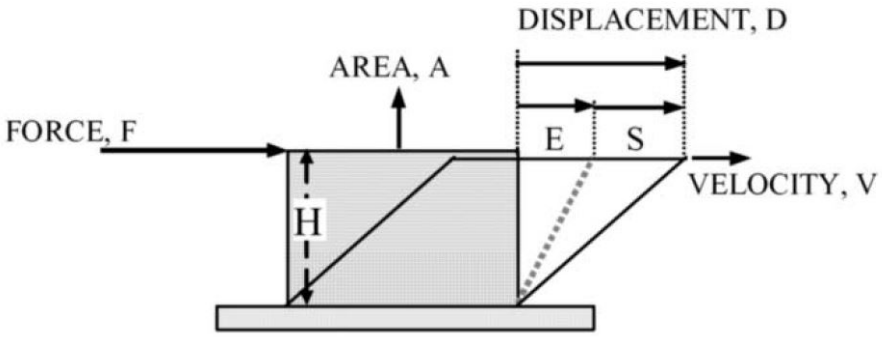

Figure 4.4: Diagram of a small cubical volume of height, H, in shear. The displacement, D, due to deformation is composed of two parts: an elastic part, E, and a slippage part, S. With constant force F, E remains constant but S continues to increase. When F is removed, E diminishes to zero and S remains [21].

Equations (3.5) and (3.6). For a given temperature, pressure and composition, μ, the dynamic viscosity, is the constant of proportionality in this relationship [11].

4.3.1 Generalized Newtonian Models

This set of equations is commonly used to describe non-Newtonian behaviour, taking into account the fact that viscosity changes with shear rate for some fluids, such as blood. In Generalized Newtonian Models (GNM), if the viscosity is to depend on the tensor **D**, then it must depend on its invariants, $I_{\mathbf{D}}, II_{\mathbf{D}}$ and $III_{\mathbf{D}}$,the first to third principal invariants of the strain rate tensor:

$$I_{\mathbf{D}} = tr\mathbf{D} \tag{4.1}$$

$$II_{\mathbf{D}} = \frac{1}{2}((tr\mathbf{D})^2 - tr(\mathbf{D}^2)) \tag{4.2}$$

$$III_{\mathbf{D}} = det(\mathbf{D}) \tag{4.3}$$

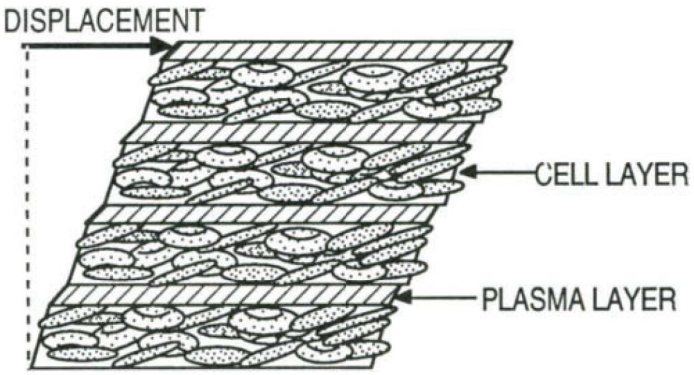

Figure 4.5: Formation of compacted cell layers separated by plasma layers [21].

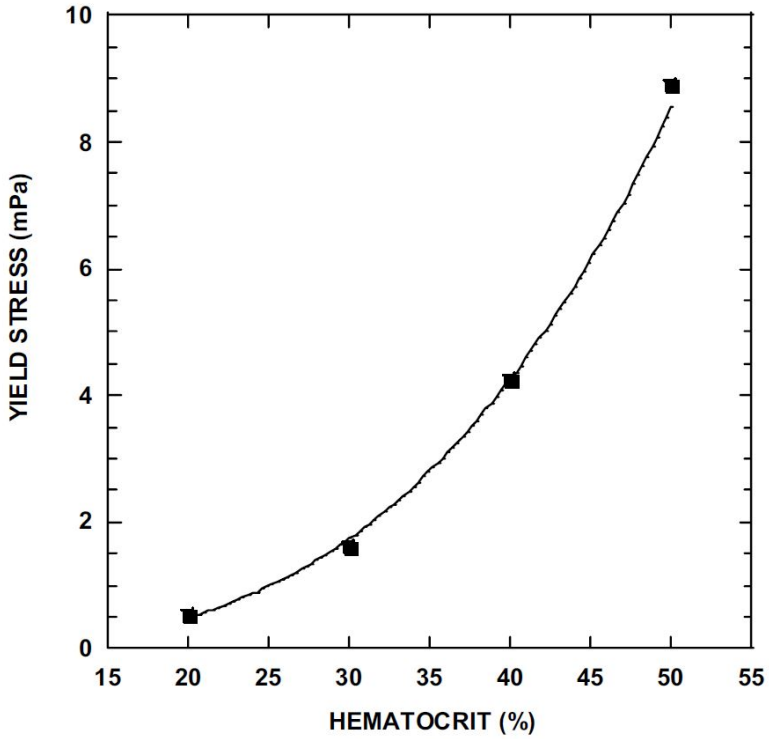

Figure 4.6: Effect of haematocrit on the yield stress of blood [8].

For incompressible fluids $I_{\mathbf{D}}$ is equal to zero and for most real fluids $III_{\mathbf{D}}$ is practically zero. If the shear rate denoted by $\dot{\gamma}$ is defined as:

$$\dot{\gamma} = \sqrt{2tr(\mathbf{D}^2)} = \sqrt{-4II_{\mathbf{D}}} \tag{4.4}$$

the negative sign under the square root due to the second invariant being negative. Then, the stress tensor for a generalized Newtonian model can be written in the form of:

$$\boldsymbol{\tau} = 2\mu(\dot{\gamma})\mathbf{D} \tag{4.5}$$

where $\mu(\dot{\gamma})$ is a shear rate dependent viscosity function [24, 25].

There are many popular GNMs used to describe the non-Newtonian properties of blood. The Power-Law model is one of such models where the viscosity function is given by

$$\mu(\dot{\gamma}) = m\dot{\gamma}^{n-1} \tag{4.6}$$

where m and n are positive constants. This model has the Newtonian fluid as a particular case when n has a unit value. When $n < 1$ the models shows shear-thinning behaviour while for values of $n > 1$ the viscosity increases with shear rate, thus leading to shear thickening fluids.

Another branch of models are the ones with viscosity functions that can be written in the general form of:

$$\mu(\dot{\gamma}) = \mu_\infty + (\mu_0 - \mu_\infty)F(\dot{\gamma}), \tag{4.7}$$

where $F(\dot{\gamma})$ is a shear rate dependent function, particular to each model, that satisfies the conditions

$$\lim_{\dot{\gamma}\to 0} F(\dot{\gamma}) = 1 \tag{4.8}$$

$$\lim_{\dot{\gamma}\to \infty} F(\dot{\gamma}) = 0 \tag{4.9}$$

It is important to note that the values of these parameters for blood modeling are highly dependent on temperature[25]. Cho and Kensey [26] propose the following values for ρ_f, μ_0 and μ_∞ at a temperature of 37 [ºC]: $\rho_f = 1056\ [kg/m^3]$, $\mu_0 = 0.056\ [Pa{\cdot}s]$, $\mu_\infty = 0.00345\ [Pa{\cdot}s]$.

Table 4.1 shows some of the shear rate dependent functions along with the corresponding models.

Table 4.1: Generalized Newtonian models for blood

Model	$\frac{\mu(\dot{\gamma})-\mu_\infty}{\mu_0-\mu_\infty} = F(\dot{\gamma})$
Powell-Eyring	$\frac{sinh^{-1}(\lambda\dot{\gamma})}{\lambda\dot{\gamma}}$
Cross	$\frac{1}{1+(\lambda\dot{\gamma})^m}$
Modified Cross	$\frac{1}{[1+(\lambda\dot{\gamma})^m]^a}$
Carreau	$[1+(\lambda\dot{\gamma})^2]^{\frac{n-1}{2}}$
Carreau-Yasuda	$[1+(\lambda\dot{\gamma})^a]^{\frac{n-1}{a}}$

Provided that the $\mu(\dot{\gamma})$ function gives a good description of the viscosity data, care still has to be taken in order to get reliable and accurate results. Bird [24] recommends GNMs to be used in steady flow in conduits of constant cross section or in systems close to steady-state. These models should not be used in flows such as blood flow, that change rapidly with time.

4.3.2 Viscoelastic Models

None of the characteristic models presented in the previous sections are able to portray the viscoelastic response of blood. Most viscoelastic models derive from the idea to combine viscosity and elasticity, the latter through Hooke's law of elasticity [24]. In fact, the first attempt at a simple linear viscoelastic constitutive equation is attributed to the Maxwell model, defined by:

$$\boldsymbol{\tau} + \lambda \frac{\partial \boldsymbol{\tau}}{\partial t} = 2\mu \mathbf{D} \tag{4.10}$$

where λ is a time constant called the relaxation time. Figure 4.7 shows a schematic representation of the mechanical analogue for this linear model.The spring represents the elastic component, while the damper represents the viscous forces. $\boldsymbol{\tau}$ is the total force, an analogue for the stress tensor, given by $\boldsymbol{\tau} = \gamma_v \mu + \gamma_e G$. The relaxation time λ is given by the ratio between viscosity μ and elastic modulus G [24].

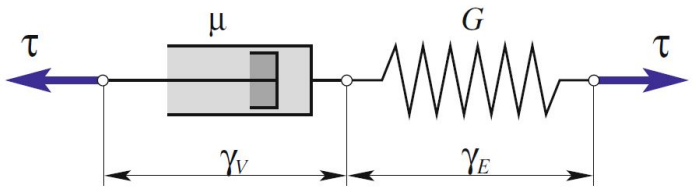

Figure 4.7: Mechanical analogue of the Maxwell model [25].

Viscoelastic fluids obey the constitutive equation of linear viscoelasticity for small strains. However this equation is not valid for deformations of arbitrary magnitude and rate, since it violates the principal of frame invariance [23]. More general constitutive equations, not restricted by the factors above mentioned, can be obtained by modifying linear viscoelastic models. These models obtained by replacing the time derivatives by convected derivatives,$\delta/\delta t$, are called *quasi-linear* models [24]. This would allow the model to be made frame invariant, meaning that the response of the material is not affected by its location and orientation [23].

The *upper-convected derivative* is defined by:

$$\frac{\delta \mathbf{A}}{\delta t} = \overset{\triangledown}{\mathbf{A}} = \frac{D\mathbf{A}}{Dt} - \mathbf{L}\mathbf{A} - \mathbf{A}\mathbf{L}^T \tag{4.11}$$

with:

$$\mathbf{L} = \nabla \mathbf{u} + \nabla \mathbf{u}^T = 2\mathbf{D} \tag{4.12}$$

and where:

$$\frac{D\mathbf{A}}{Dt} = \frac{\partial \mathbf{A}}{\partial t} + \frac{\partial \mathbf{A}}{\partial \mathbf{x}} \frac{d\mathbf{x}}{dt} \tag{4.13}$$

is the material time derivative. The Maxwell model in Equation (4.10) can now be reinterpreted as the upper-convected Maxwell model (UCM):

$$\boldsymbol{\tau} + \lambda \overset{\triangledown}{\boldsymbol{\tau}} = 2\mu \mathbf{D}. \tag{4.14}$$

Oldroyd's proposal is the combination of the Newtonian and the Maxwell models, through the sum of the respective solvent and elastic (or polymer) stresses. If once again we take into consideration a physical approach, the junction can be said to be in parallel as seen in Figure 4.8.

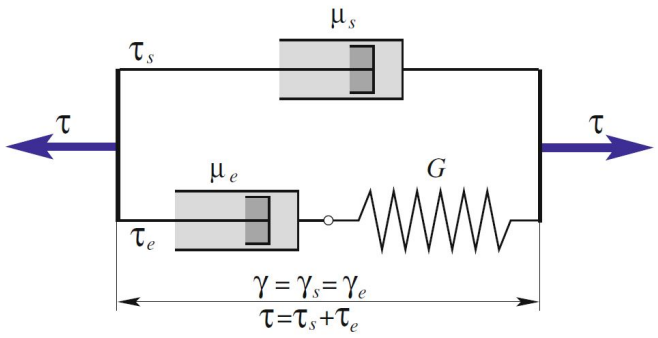

Figure 4.8: Mechanical analogue of an Oldroyd-type model [25].

Here, the total force $\boldsymbol{\tau}$ is expressed as the sum of solvent $\boldsymbol{\tau}_s$ and the elastic $\boldsymbol{\tau}_e$ contributions, as an analogue to the decomposition of the stress tensor $\boldsymbol{\tau}$:

$$\boldsymbol{\tau} = \boldsymbol{\tau}_s + \boldsymbol{\tau}_e = 2\mu_s \mathbf{D} + \boldsymbol{\tau}_e \tag{4.15}$$

where $\boldsymbol{\tau}_e$, the elastic stress, satisfies the UCM equation:

$$\boldsymbol{\tau}_e + \lambda \overset{\triangledown}{\boldsymbol{\tau}}_e = 2\mu_e \mathbf{D} \tag{4.16}$$

Taking into account the total stress $\boldsymbol{\tau}$, the model can be rewritten as:

$$\boldsymbol{\tau} + \lambda_1 \overset{\triangledown}{\boldsymbol{\tau}} = 2\mu(\mathbf{D} + \lambda_2 \mathbf{D}) \tag{4.17}$$

where $\lambda_1 = \lambda$ is the relaxation time, $\mu = \mu_s + \mu_e$ is the total viscosity and $\lambda_2 = \lambda\mu_s/\mu$ is the retardation time. The model in Equation (4.17) is called Oldroyd-B model. This type of fluid can be considered as a Maxwell fluid with additional viscosity [25].

This constitutive equation, in a steady state shear flow, predicts a constant viscosity, a first normal stress difference quadratic in the shear rate, and a zero second normal stress difference [11]. The simplicity in the constitutive equation of Oldroyd models gives them great utility. However it brings about poor approximation to some material functions, such as the prediction of an infinite

stress at a finite elongational rate, which is not physically realistic [24]. Another downside of the Oldroyd-B model is that it accounts for the viscoelasticity of blood but not for its shear-thinning behaviour as in Generalized Newtonian equations.

There are, however, other ways to obtain non-linear viscoelastic constitutive equations that more accurately represent real material data. The generalized Oldroyd-B (GOB) constitutive equations introduce a modification to the previous model, including a dependence of the solvent viscosity on the second invariant of the strain rate tensor, i.e., as seen in GNMs a dependence on the shear rate $\dot{\gamma}$ [25]:

$$\boldsymbol{\tau}_s = 2\mu_s(\dot{\gamma})\mathbf{D} \tag{4.18}$$

The viscosity function can be, for example, any of the ones introduced in Table 4.1.

Another manner to achieve the non-linearity in a model is the inclusion of non-linear stress terms. Such is the case of the Giesekus model.

$$\boldsymbol{\tau} = \boldsymbol{\tau}_s + \boldsymbol{\tau}_e \tag{4.19}$$

$$\boldsymbol{\tau}_s = 2\mu_s\mathbf{D} \tag{4.20}$$

$$\boldsymbol{\tau}_e + \lambda\overset{\triangledown}{\boldsymbol{\tau}}_e + \frac{\alpha\lambda}{\mu_e}(\boldsymbol{\tau}_e \cdot \boldsymbol{\tau}_e) = 2\mu_e\mathbf{D} \tag{4.21}$$

The Giesekus model has an additional parameter, the mobility factor α, and it is a constitutive equation based on anisotropic drag [23]. It differs from the UCM equation by the quadratic term in stress. It is the inclusion of this term $(\boldsymbol{\tau}_e \cdot \boldsymbol{\tau}_e)$ that results in more realistic material functions [24].

This is a shear-thinning viscoelastic model, capable of predicting steady-state shear viscosity and first and second normal stress differences [23]. It is important to note however, that the introduction of a non-zero second normal stress difference, is not coherent with what has so far been reported for blood [27].

Along with the non-linear models above mentioned there is also another category called the network models, that can fit data in extensional as well as shear flow [23]. The Phan-Thien/Tanner (PTT) constitutive equation falls under this category and is defined by:

$$\boldsymbol{\tau} = \boldsymbol{\tau}_s + \boldsymbol{\tau}_e \tag{4.22}$$

$$\boldsymbol{\tau}_s = 2\mu_s \mathbf{D} \tag{4.23}$$

$$f(\boldsymbol{\tau}_e)\boldsymbol{\tau}_e + \lambda \overset{\square}{\boldsymbol{\tau}}_e = 2\mu_e \mathbf{D} \tag{4.24}$$

where $\square$ is the symbol for the Gordon-Schowalter convected derivative and $f(\boldsymbol{\tau}_e)$ is a specified function with two different possibilities:

$$f(\boldsymbol{\tau}_e) = 1 + \frac{\lambda\varepsilon}{\mu_e} tr(\boldsymbol{\tau}_e) \tag{4.25}$$

$$f(\boldsymbol{\tau}_e) = \exp\left(\frac{\lambda\varepsilon}{\mu_e} tr(\boldsymbol{\tau}_e)\right) \tag{4.26}$$

ε being the extensibility coefficient. The PTT model with the linear choice for $f(\boldsymbol{\tau}_e)$, Equation (4.25), is similar in its prediction to the Giesekus equation, with the exception that the linear PTT model has a zero second normal stress difference [23, 12].

By replacing of the Gordon-Schowalter convected derivative with the upper-convected derivate while using the linear form of $f(\boldsymbol{\tau}_e)$ we get the simplified PTT model or sPTT. This simplified equation is generally more popular due to the unphysical oscillations in μ that the Gordon-Schowalter convected derivative brings about, which may be confused with numerically induced oscillations [23].

All of the non-linear models presented have the shortcoming of having a single relaxation time. A common approach to remedy this problem that can be used in any of the non-linear differential constitutive equations, shown in Table 4.2, is the use of multiple modes, each with different time constants [24].

Table 4.2: Multi-mode forms of the viscoelastic models

Model	$\boldsymbol{\tau}_s$	$\boldsymbol{\tau}_e = \sum_{k=1}^{m} \boldsymbol{\tau}_{e_k}$
Oldroyd-B		$\boldsymbol{\tau}_{e_k} + \lambda_k \overset{\triangledown}{\boldsymbol{\tau}}_{e_k} = 2\mu_{e_k}\mathbf{D}$
Giesekus	$2\mu_s\mathbf{D}$	$\boldsymbol{\tau}_{e_k} + \lambda_k \overset{\triangledown}{\boldsymbol{\tau}}_{e_k} + \frac{\alpha_k\lambda_k}{\mu_{e_k}}(\boldsymbol{\tau}_{e_k}\cdot\boldsymbol{\tau}_{e_k}) = 2\mu_{e_k}\mathbf{D}$
sPTT		$f(\boldsymbol{\tau}_{e_k})\boldsymbol{\tau}_{e_k} + \lambda_k \overset{\triangledown}{\boldsymbol{\tau}}_{e_k} = 2\mu_{e_k}\mathbf{D}$

Summarizing the above description, there are three different models that will be given a further in-depth analysis: the Generalized Oldroyd-B and the multi-mode Giesekus and simplified Phan-Thien/ Tanner models. All these models are capable of depicting non-linear viscoelasticity along with the shear-thinning properties of blood and will be used in numerical simulations. Haemodynamic results using these models will be compared with those obtained by the more popular Newtonian (NS) and Generalized Newtonian (GNM) models, in order to move in the direction of more accurate rheological models for blood.

Chapter 5

Methodology

The present chapter deals with the methodology applied to all the three-dimensional numerical simulations performed using ANSYS Fluent. The before mentioned viscoelastic models are not included in the software but they can be implemented through the use of user-defined functions (UDFs). The meshing was done using the ANSYS Meshing meshing tool. A series of simulations were done in idealized geometries in order to simplify the interpretation and study of the different rheological models.

5.1 Implementation in Fluent

ANSYS Fluent is one of the most popular commercial solvers for CFD applications. Due to the commercial nature of the software, the only way to modify the governing equations is through the inclusion of additional source code according to ANSYS Fluent requirements. The extra elastic stress components and their respective transport equations will thus be treated as a series of partial differential equations (PDEs) while the tensor's gradient will be added as a source term in the Navier-Stokes momentum equations in Equation (3.8).

It is important to note that this implementation translates in an additional set of equations, one for each component of the stress tensor, that will have to be calculated. In particular, when using this approach to model the multi-mode constitutive equations, there will be a high increase in computational load.

5.1.1 UDFs

User-Defined Functions, or UDFs, are functions or subroutines that can be loaded with ANSYS Fluent allowing the enhancement of the solver's features. UDFs are programmed in a modified C language and they are defined using macros provided by ANSYS Fluent that allow access to the solver data as well as other functions.

These functions allow for the customization of a large amount of features such as boundary conditions and scalar transport equations. Both types of UDF are used in the setups for the numerical simulations although only the latter being the main focus of this thesis.

In the interest of understanding how to implement the viscoelastic models of Chapter 4, these models can be compactly written as:

$$\tau_{ij} = \tau_{ij_s} + \tau_{ij_e} \tag{5.1}$$

$$\tau_{ij_s} = 2\mu_s D_{ij} \tag{5.2}$$

$$\tau_{ij_e} = \sum_{k=1}^{m} \tau_{ij_k} \tag{5.3}$$

with

$$f(\tau_{ij_k})\tau_{ij_k} + \lambda_k \overset{\triangledown}{\tau}_{ij_k} + \alpha_k \frac{\lambda_k}{\mu_{e_k}} (\tau_{in_k} \cdot \tau_{nj_k}) = 2\mu_{e_k} D_{ij} \tag{5.4}$$

where

$$f(\tau_{ij_k}) = 1 + \frac{\lambda_k \varepsilon_k}{\mu_{e_k}} tr(\tau_{ij_k}) \tag{5.5}$$

In Equation (5.3) the number of modes in the constitutive equations is referred to as m. In this work the Oldroyd-B viscoelastic model implemented shows only a single mode, leading to $m = 1$. In the case of both the multi-mode Giesekus and sPTT models m is equal to 4.

Adjusting the coefficients α_k and ε_k in each mode as described in Table 5.1, it is possible to get the different constitutive equations. Here the PTT models come as an exception, as only the linear simplified one is represented.

Table 5.1: Coefficients for the different viscoelastic constitutive equations

Model	α_k	ε_k
Oldroyd-B	0	0
Giesekus	–	0
sPTT	0	–

Using the definition of the upper convected derivative in Equation (4.11), while using Einstein notation for compactness, the following is achieved:

$$\overset{\triangledown}{\tau}_{ij_k} = \frac{\partial \tau_{ij_k}}{\partial t} + u_n \frac{\partial \tau_{ij_k}}{\partial x_n} - \tau_{nj_k} \frac{\partial u_i}{\partial x_n} - \tau_{in_k} \frac{\partial u_j}{\partial x_n} \tag{5.6}$$

Replacing Equation (5.6) in Equation (5.4) and reordering the terms, leaving only the upper convected derivative on the left side, it is possible to get:

$$\frac{\partial \tau_{ij_k}}{\partial t} + u_n \frac{\partial \tau_{ij_k}}{\partial x_n} - \tau_{nj_k} \frac{\partial u_i}{\partial x_n} - \tau_{in_k} \frac{\partial u_j}{\partial x_n} = \frac{2\mu_{e_k} D_{ij}}{\lambda_k} - \frac{1}{\lambda_k} f(\tau_{ij_k}) \tau_{ij_k} - \frac{\alpha_k}{\mu_{e_k}} (\tau_{in_k} \cdot \tau_{nj_k}) \tag{5.7}$$

These stress components can now be added to the solver as User-Defined Scalars (UDS) transport equations. The scalar equations are solved by Fluent after defining the diffusion coefficient, and the convective flux and unsteady terms. As there is no diffusion term present in the viscoelastic models, after setting this parameter to zero in Fluent, by default any UDS comes in the form of:

$$\frac{\partial \phi_k}{\partial t} + u_n \rho \frac{\partial \phi_k}{\partial x_n} = S_{\phi_k} \qquad where \quad k = 1, ..., N \;\; scalars \tag{5.8}$$

with $\frac{\partial \phi_k}{\partial t}$ being the unsteady term and $u_n \rho \frac{\partial \phi_k}{\partial x_n}$ the convected term, solved in Fluent to obtain user-defined scalars. To allow the fitting of the viscoelastic models in this way there is a need to modify the convected coefficient, $u_n \rho$, for it to match the one in Equation (5.7), i.e., changing the coefficient to u_n. This customization can be achieved through another UDF function that will be later activated in the UDS window in Fluent.

If Equation (5.7) is once more rearranged, it can now be applied in the form of Equation (5.8) where:

$$\frac{\partial \tau_{ij_k}}{\partial t} + u_n \frac{\partial \tau_{ij_k}}{\partial x_n} = S_{\tau_{ij_k}} \tag{5.9}$$

and the sources are defined for each stress component, and for each mode, as:

$$S_{\tau_{ij_k}} = \frac{2\mu_{e_k} D_{ij}}{\lambda_k} - \frac{1}{\lambda_k} f(\tau_{ij_k}) \tau_{ij_k} - \frac{\alpha_k}{\mu_{e_k}} (\tau_{in_k} \cdot \tau_{nj_k}) + \tau_{nj_k} \frac{\partial u_i}{\partial x_n} + \tau_{in_k} \frac{\partial u_j}{\partial x_n} \tag{5.10}$$

As the elastic stress tensor for the constitutive equations is symmetric over the diagonal, that is, $\tau_{ij_k} = \tau_{ji_k}$, for a three-dimensional case there is only the need to calculate six components for each mode.

The last step is now to analyse the Navier-Stokes equations, through the modification of the basic conversion of momentum equation, Equation (3.8), as to include the decomposition of stress tensor $\boldsymbol{\tau}$. The solvent contribution, $\boldsymbol{\tau}_s$, is already included and is the one generally calculated by Fluent, either with constant viscosity or with a shear dependent one. As such there is only the need to account for the elastic parts of the stress, that were already calculated as scalars. This can be achieved through the addition of the divergence of the extra stress tensor $\boldsymbol{\tau}_e$ as sources to the momentum equations, known in Fluent as momentum sources.

$$S_{M_x} = \sum_{k=1}^{m} \frac{\partial \tau_{xn_k}}{\partial x_n} \tag{5.11}$$

$$S_{M_y} = \sum_{k=1}^{m} \frac{\partial \tau_{yn_k}}{\partial x_n} \tag{5.12}$$

$$S_{M_z} = \sum_{k=1}^{m} \frac{\partial \tau_{zn_k}}{\partial x_n} \tag{5.13}$$

5.1.2 Blood properties and model parameters

Blood was considered an isotropic, homogeneous, non-Newtonian viscoelastic fluid with a constant density [28], ρ_f, of 1056 $[kg/m^3]$. The viscoelastic models were first directly compared to a purely Newtonian solution (NS) with a constant viscosity $\mu_f = 0.00345[Pa \cdot s]$ and to a purely shear-thinning one. The Carreau model shown in Table 4.1 was used to account for this behaviour. Blood can be fitted to this model with the parameters in Section 4.3.1 along with a relaxation time, λ, of 3.313 $[s]$ and a characteristic constant of the flow, n, of 0.3568 [26, 5].

Numerical simulations for the Generalized Oldroyd-B model (GOB) were performed using the already introduced Carreau model for the solvent viscosity, as well as the following parameters for the elastic components [29]: $\mu_e = 4.0 \times 10^{-6}$ $[Pa \cdot s]$ and $\lambda_1 = 0.06$ $[s]$. Once again, it is important to note that the GOB constitutive equation used is not a multi-mode one, thus only having a single combination of parameters.

The viscoelastic Giesekus and sPTT models were both implemented in multi-mode form with the corresponding fits by Campo-Deano [27], shown in Table 5.2.

Table 5.2: Parameters of the multi-mode Giesekus and sPTT model fits for whole human blood [27]

	Giesekus			sPTT		
Mode	μ_{e_k} $[Pa \cdot s]$	λ_k $[s]$	α_k	μ_{e_k} $[Pa \cdot s]$	λ_k $[s]$	ε_k
1	0.05	7	0.06	0.05	7	0.2
2	0.001	0.4	0.001	0.001	0.4	0.5
3	0.001	0.04	0.001	0.001	0.4	0.5
4	0.0016	0.006	0.001	0.0016	0.006	0.5
Solvent	$\mu_s = 0.0012$ $[Pa \cdot s]$			$\mu_s = 0.0012$ $[Pa \cdot s]$		

5.2 Idealized Geometry

The first numerical simulations were performed to model blood flow in three-dimensional idealized geometries of right coronary arteries. Particularly, the bifurcation zone was chosen, as the

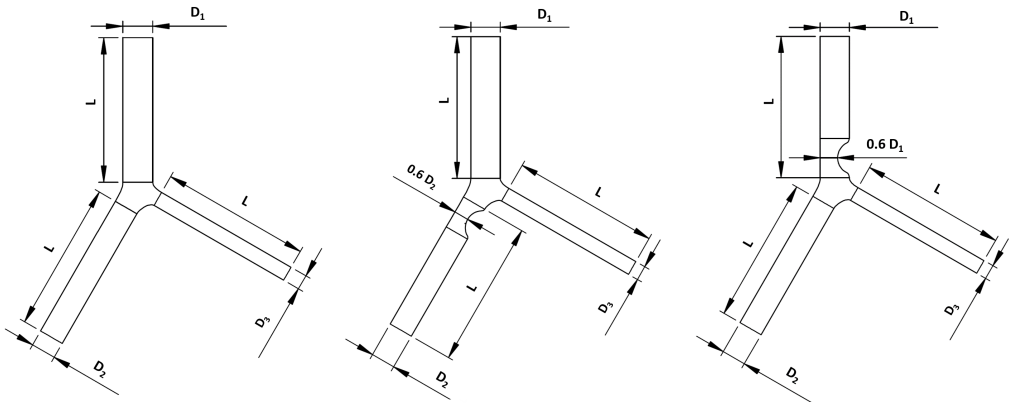

Figure 5.1: Idealized vessels.

flow separation that occurs here would lead to higher velocity gradients. Three geometries were used in order to achieve different flow behaviour. One is an asymmetric bifurcation, with the remaining geometries being of stenosed arteries only differing in the location of the stenosis. In one geometry the stenosed region is located after the bifurcation, as in the remaining one the stenosis is present before the junction. All geometries share common parameters that were specified for the parent and daughter vessels, such as branching angles, diameters and lengths.

The 2D schematics, taken along the middle plane for the different geometries, are shown in Figure 5.1 where $D_1 = 3$ $[mm]$, $D_2 = 2.5$ $[mm]$ and $D_3 = 1.5$ $[mm]$. The length for every branch is five times the diameter of the parent vessel, $L = 5 \times D_1$, while both stenosed regions correspond to a 40% reduction in diameter.

5.3 Mesh convergence analysis

The discretization of the fluid domain was realized using the automatic meshing algorithm existent in Workbench, ANSYS Meshing. All the geometries were meshed as seen in Figure 5.2, using the Tetrahedrons Patch Independent Method, as implemented by Pinho et al. [30], along with a refined mesh near the walls through the use of inflation. The need to further refine the mesh in this region comes from the main objective of this study, which is to analyse WSS haemodynamic descriptors in arterial walls.

A mesh convergence analysis was performed in order to ensure accurate and mesh independent results, as is the common practice in most CFD studies. In order to evaluate the grid performance for the meshes generated, initial simulations were made, increasing the number of elements in each mesh approximately by a factor of 2. Three meshes were generated in these tests for the idealized stenosed artery where the stenosis is present after the bifurcation. This choice is due to the increased complexity of the geometry in the throat region, in either the meshing process or the consequent flows, when compared to the simply bifurcated one. The simulations consider the multi-mode Giesekus viscoelastic model as to guarantee an appropriate behaviour when modelling the extra stress tensor.

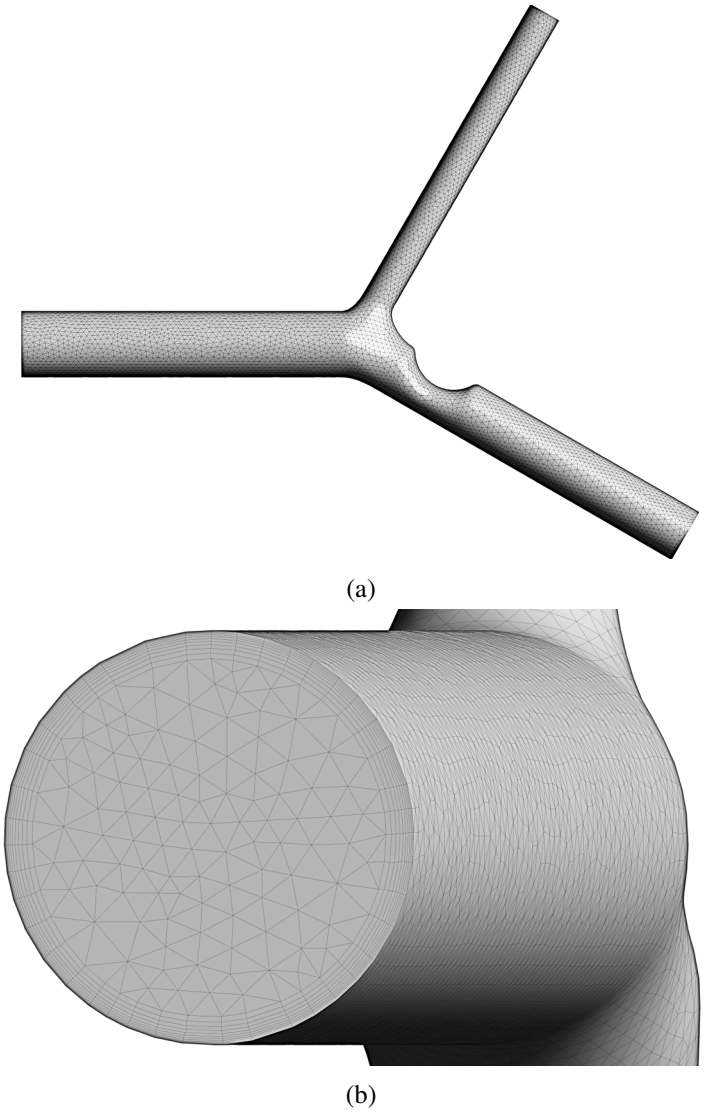

(a)

(b)

Figure 5.2: (a) Example of the mesh obtained for one of the idealized geometries with stenosis. (b) Detail of the inflation layers.

Mesh sensitivity was analysed, as by Pinho et al. [28], through the *Skewness* parameter. This is a *Mesh Quality Metric* provided by the software which refers to face proximity and the cell's angles. *Skewness* can vary from 0 to 1, where values closer to the upper limit are indicative of poor mesh quality. In Figure 5.3, results for the different meshes were also compared in terms of velocity profiles taken in the parent vessel and also after the throat region where there is the appearance of a recirculation zone. Table 5.3 provides the key mesh parameters for the meshes used.

It is possible to verify from Figure 5.3 that there is only a negligible difference in the velocity profiles for the different meshes in the first position, i.e., when in a zone with a fully developed profile. In this case, even the coarser mesh with approximately 150 000 elements shows accurate result despite it's maximum skewness value being close to the acceptable maximum of 0.9 [30].

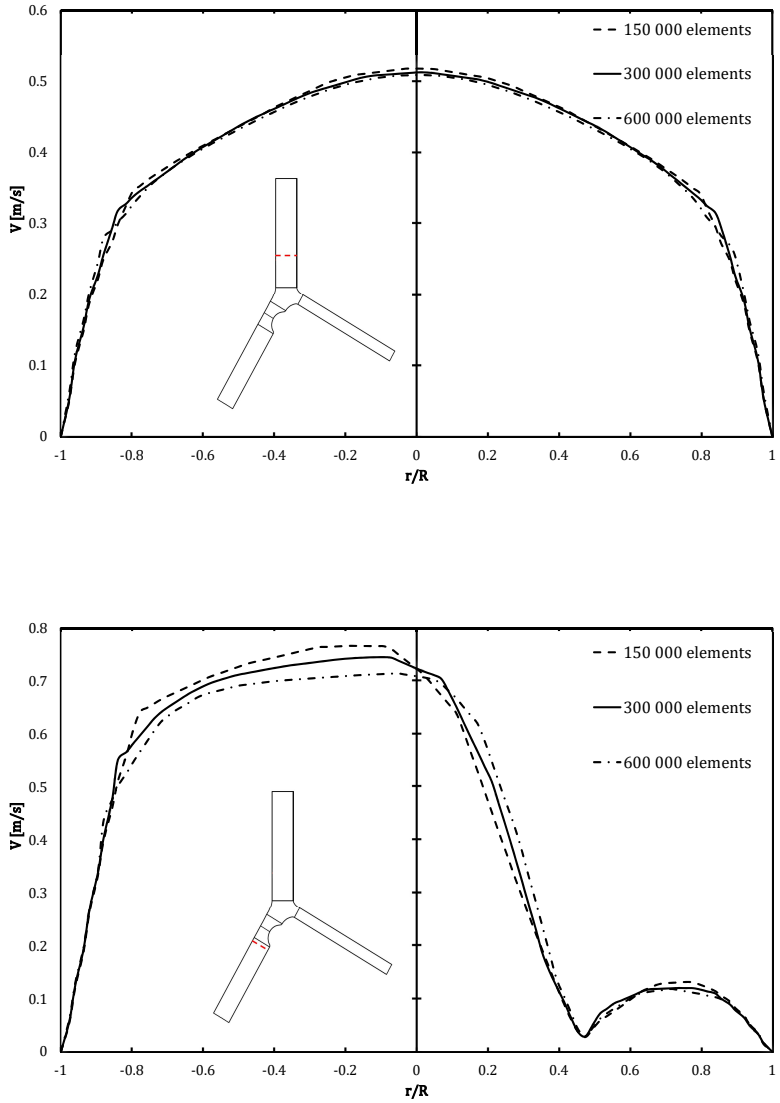

Figure 5.3: Idealized stenosed artery schematics. Red dashed lines indicate the velocity profiles' position (left). Velocity profiles along the mid plane of the artery for different mesh sizes (right).

When looking at the recirculation zone after the stenosis the results provided by the coarser mesh show a very large discrepancy from the finer meshes. In particular when away from the refined areas near the walls, there is an over-prediction of approximately 12% in the velocity fields. The behaviour for the medium mesh, 300 000 elements, is satisfactory, showing maximum deviations from the finer mesh, 600 000 elements, in the order of 5%. Taking into account the previous arguments and the reduced value for maximum skewness, the mesh with 300 000 elements was found sufficient and is used to perform the simulations.

Table 5.3: Number of elements and maximum and average Skewness for each mesh

Mesh	*#Elements*	$max_{Skewness}$	$avg_{Skewness}$
1	139 651	0.797	0.192
2	294 982	0.699	0.172
3	586 075	0.706	0.150

5.4 Boundary conditions

For the models to be solved there is a need to provide the flow parameters and appropriate boundary conditions.

With respect to boundary conditions for the modified Navier-Stokes equations, there is a need to prescribe the velocity at the inflow boundary (inlet). In this case, to simulate the pulsatile nature of blood, a time-dependent Womersley profile already described in Section 3.1.4, was implemented. The Womersley number was taken for the radius values of the geometries used, in this case $R_1 = \frac{D_1}{2} = 1.5\ [mm]$ and with a blood density $\rho_f = 1056\ [kg/m^3]$. The blood dynamic viscosity μ_f was considered equal to 0.00345 $[Pa \cdot s]$ and the cardiac frequency was calculated for a period T of 0.74 $[s]$ (the total time of the cardiac cycle) such that $\omega_f = \frac{2\pi}{T} = 8.48\ [rad/s]$. This resulted in a velocity profile with a Womersley number (Wo) equal to 2.40. For the outflow boundary condition a time-varying pressure profile was imposed, simulating the blood pressure during a cardiac cycle.

Both boundary conditions shown in Figure 5.4 have usual values for right coronary arteries and were implemented and added to Fluent as UDFs, as by Pinho et al. [3].

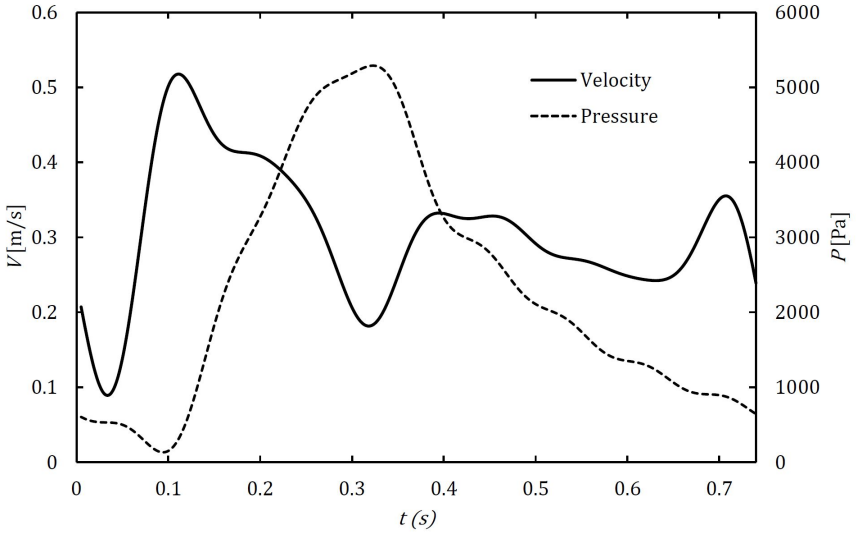

Figure 5.4: Mean time-dependent velocity imposed at the inlet and time-dependent pressure profile imposed at the outlets.

On the vessel walls homogeneous Dirichlet conditions were imposed for the velocity, i.e., no-slip condition, expressing that the velocity at the wall is the wall velocity (stationary). This is appropriate due to the consideration of rigid walls.

The extra stresses for the viscoelastic models also need the prescription of boundary conditions. Homogeneous Neumann boundary conditions are imposed for the components of the extra stress tensor at all boundaries.

5.5 Numerical methods

A finite element approach has been adopted for the numerical solution of the blood flow models. As already discussed, all the numerical simulations were performed in Workbench ANSYS, with the Fluent software in double precision mode. No parallel computations have been performed due to the extensive use of UDFs. The CFD model was set up for unsteady flow due to the time-dependent nature of the models at hand. At each time-step ($5 \times 10^{-3}[s]$) the velocity-pressure coupled equations were solved with the SIMPLE algorithm. The momentum and UDS equations were discretized by the second order upwind scheme. A convergence criteria of 1×10^{-4} was used.

Chapter 6

Results and discussion

The models described in Section 4.3.2 were used to investigate the influence of shear-thinning and viscoelastic effects on the behaviour of blood flow in different idealized geometries, under physiological conditions. To further highlight these effects, the solution for the Newtonian and Generalized Newtonian models were also obtained, under the same conditions. They are used as references and for direct flow comparison.

6.1 Flow Fields

Figures 6.1 to 6.3 show the axial velocity contours at the systolic peak, maximum velocity of the cardiac cycle, taken in the symmetry plane for the five different rheological models, in each geometry.

A simple analysis of the flow fields allows for the identification of common characteristics of fluid flows in asymmetric bifurcations. By observing the simpler geometry in Figure 6.1, it is possible to see that the flow divides in two streams at the divider, forming a boundary layer at the inner walls of each daughter vessel. This is due to each diving stream turning a corner of finite radius of curvature when entering the respective secondary vessel and gaining characteristics of flow in curved vessels, i.e., faster moving flows at the outer walls. It is also possible to see the occurrence of flow separation in the branch with a smaller diameter. The sharper angle at the outer wall of the branch along with the larger flow rate in the other daughter vessel being the cause of this separation [31]. The appearance of stenosed regions as seen in the geometries of Figures 6.2 and 6.3 will also result in additional recirculation zones. In fact, in the case where the stenosis is located right before the bifurcation, this will lead to very complex flows and to an increase of the recirculation region. As expected, at the neck of the stenosis there is also flow acceleration, explaining the disparities in maximum velocity between the stenosed and non-stenosed geometries. This flow acceleration induces a reduction in the local pressure and in cases of higher grades of stenosis (larger reduction of the cross-section area) the pressure can be lower than the external pressure. In extreme cases, this effect results in the collapse of the arteries [31].

By looking into the different rheological models, the Newtonian flow shows higher velocity values across the different geometries when compared to the non-Newtonian and viscoelastic models. Whereas the multi-mode Giesekus and simplified Phan-Thien/ Tanner flows result in overall lower velocities.

6.2 Direct Flow Differences and Comparison

To gain further insight into the behaviour of the different constitutive models and allow for easier comparison, the direct difference between each pair of solutions where plotted. To emphasize the flow regions where the solutions are similar, grey colours where used in custom colour scales (with physical units in $[m/s]$), while warm and cold colours represent large differences in the solutions. As the results shown for the different geometries have been found coherent, the idealized artery with a stenosed region after the bifurcation was chosen for the analysis while the remaining plots can be found in Appendix A.

Viscoelastic and shear-thinning effects can be observed in Figure 6.4 where the Newtonian solution (NS) was subtracted to the Carreau, Generalized Oldroyd-B (GOB), Giesekus and simplified Phan-Thien/ Tanner (sPTT) models. The shear-thinning effects become evident when comparing the Carreau and the Newtonian solutions (Figure 6.4a). The axial velocity is slower in the core regions (negative difference) of the flow, due to this being a region of low shear rate, and faster (positive difference) or similar (grey areas) near the walls. The non-Newtonian shear-thinning effects become less evident with the increase of shear rate close to the walls as the viscosity becomes close to the value μ_∞ - equal to the characteristic viscosity chosen for the Newtonian case.

The combined viscoelastic and shear-thinning effects can be depicted by observing the differences between the viscoelastic models and the Newtonian solution. The similarity between the subtracted GOB and NS models (Figure 6.4b), and the Carreau and NS models (Figure 6.4a), seems to indicate that shear-thinning effects in the solvent contribution of the Generalized Oldroyd-B model are more pronounced than the viscoelastic ones.

When looking into the case of the differences between the Giesekus and sPTT models with respect to the Newtonian flow (Figure 6.4c and d), these show a similar behaviour before the bifurcation (and the stenosis). However, the impact of the viscoelasticity in the flow is clearly present in the regions after the bifurcation, where there are higher velocity gradients and the elastic extra stress tensor, $\boldsymbol{\tau_e}$, contributes to flow acceleration/deceleration [32]. The recirculation region after the stenosis is also larger for Newtonian flow. Both the shear-thinning and viscoelastic fluid behaviour tend to reduce this region [32], as seen due to the presence of higher velocities.

A more detailed comparison of the implemented viscoelastic models can be obtained when looking into the differences between all the non-Newtonian models in Figure 6.5. Here the large similarity between the viscoelastic shear-thinning GOB model and the purely shear-thinning Carreau model (Figure 6.5a) is confirmed. It can be concluded that the influence of viscoelasticity in GOB model is reduced. However, as it is to be expected of multi-mode solutions, the viscoelastic effects in the Giesekus and sPTT models show a greater degree of significance when compared

to the (single mode) GOB model (Figure 6.5c and d). This is, once again, especially pronounced in the regions after the bifurcation and after the stenosis, resulting in flatter velocity profiles. It is also important to note that the solutions for the Giesekus and sPTT have been found near equivalent (Figure 6.5b). As already mentioned in Section 4.3.2, and according to Campo-Deano [27], although the Giesekus model shows a better fit to the viscosity of blood, it introduces a non-zero second normal stress difference, which so far has not been reported for blood. Thus, the sPTT model becomes the best option for further applications, as will be the case in a subsequent section. Figure 6.6 represents the systolic velocity profiles taken for the non-Newtonian models before the bifurcation, at the bifurcation and after the stenosis. It is now possible to see in detail the almost complete overlap of the GOB and the shear-thinning Carreau models and of the multi-mode Giesekus and sPTT models. In the velocity profiles before the bifurcation, the increased flattening of the latter pair of models is already apparent. However when moving into the bifurcation area and the region after the stenosis the previous effect is even further denoted.

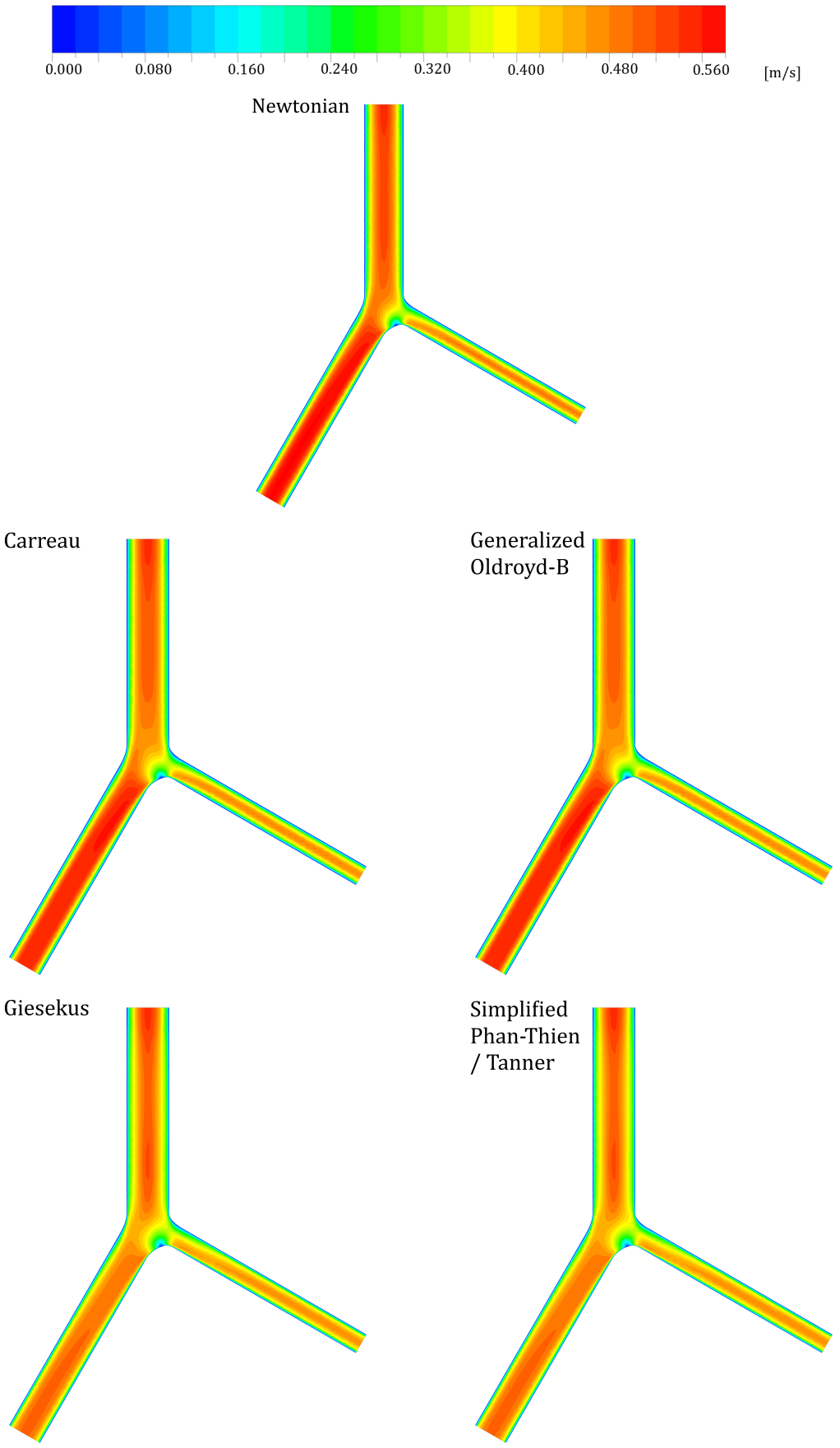

Figure 6.1: Axial velocity contours in the non-stenosed idealized right coronary artery for the different Newtonian and non-Newtonian models.

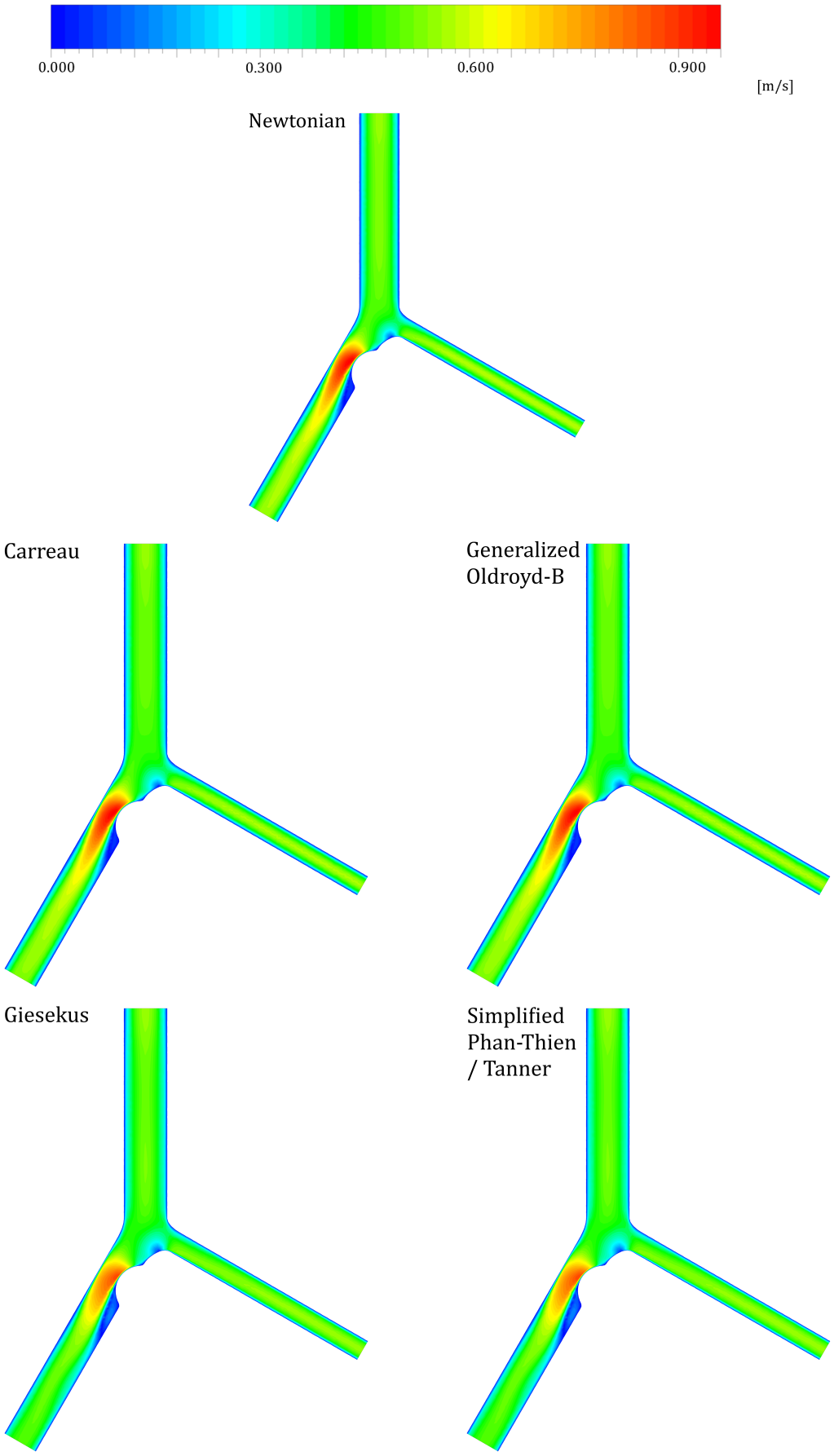

Figure 6.2: Axial velocity contours in the idealized right coronary artery with a stenosed region after the bifurcation for the different Newtonian and non-Newtonian models.

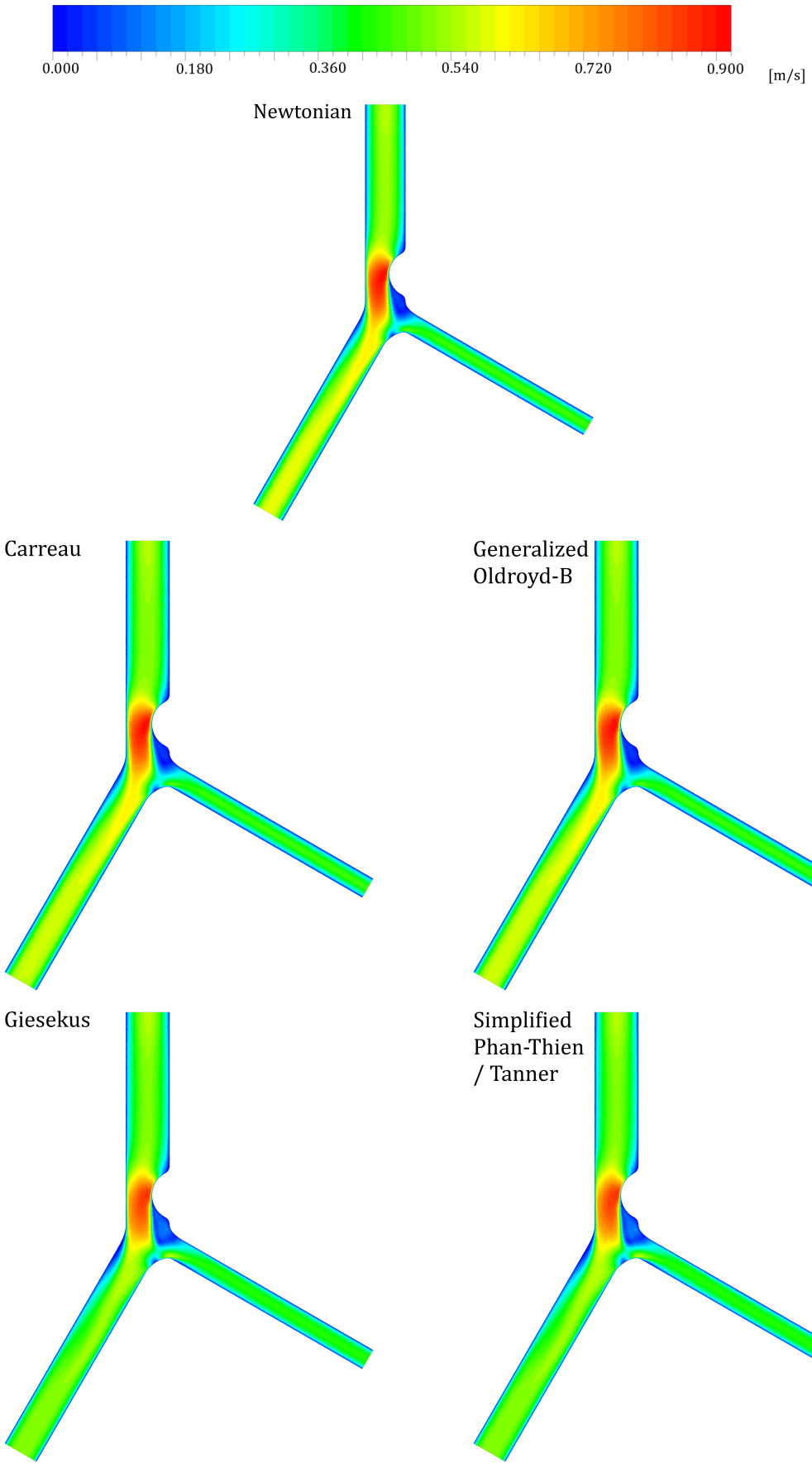

Figure 6.3: Axial velocity contours in the idealized right coronary artery with a stenosed region before the bifurcation for the different Newtonian and non-Newtonian models.

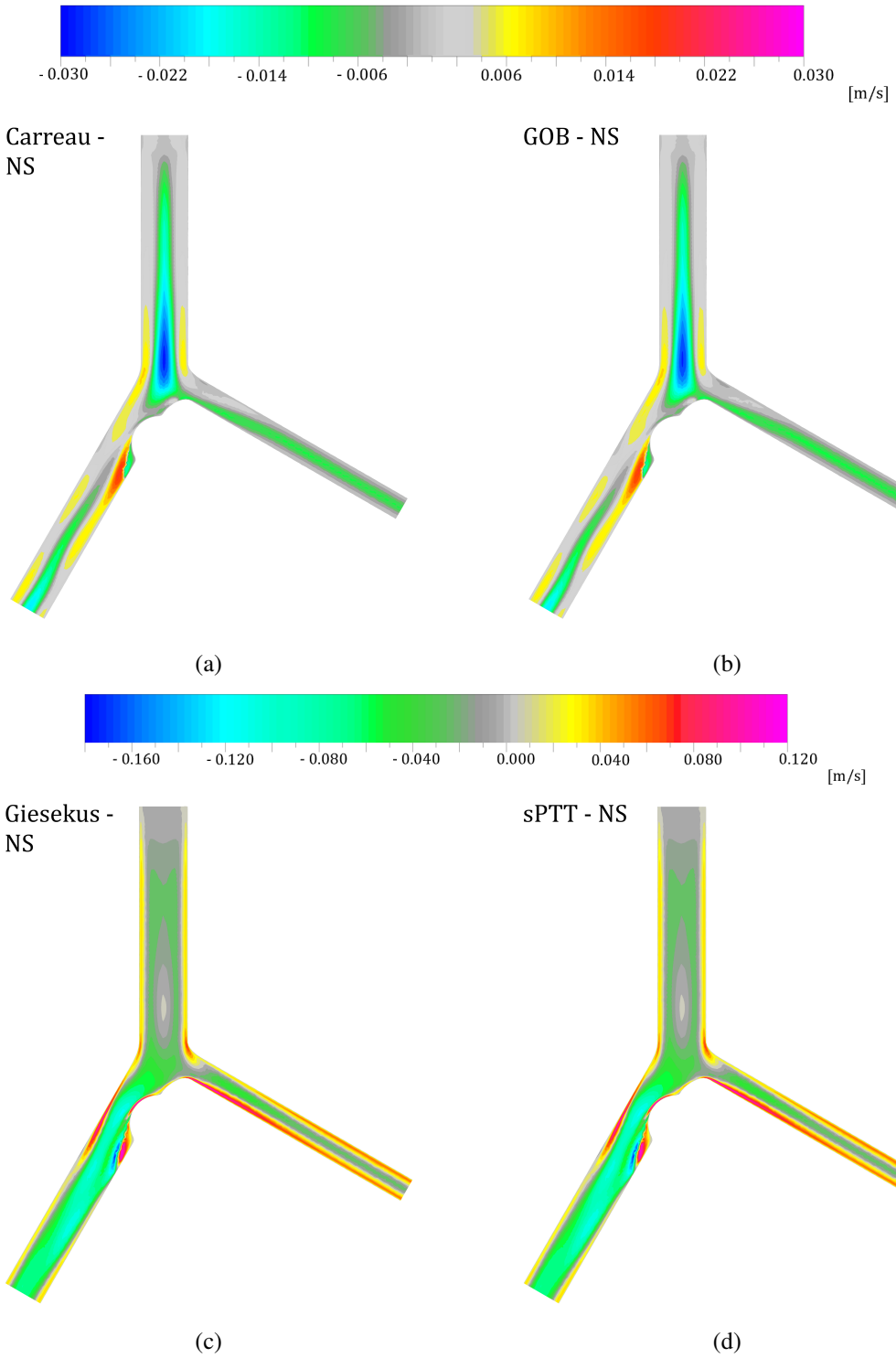

Figure 6.4: Axial velocity contours: difference between the non-Newtonian and the Newtonian solution for the idealized right coronary artery with a stenosed region after the bifurcation. (a) Difference between the Carreau and the Newtonian models. (b) Difference between the GOB and the Newtonian models. (c) Difference between the Giesekus and the Newtonian models. (d) Difference between the sPTT and the Newtonian models.

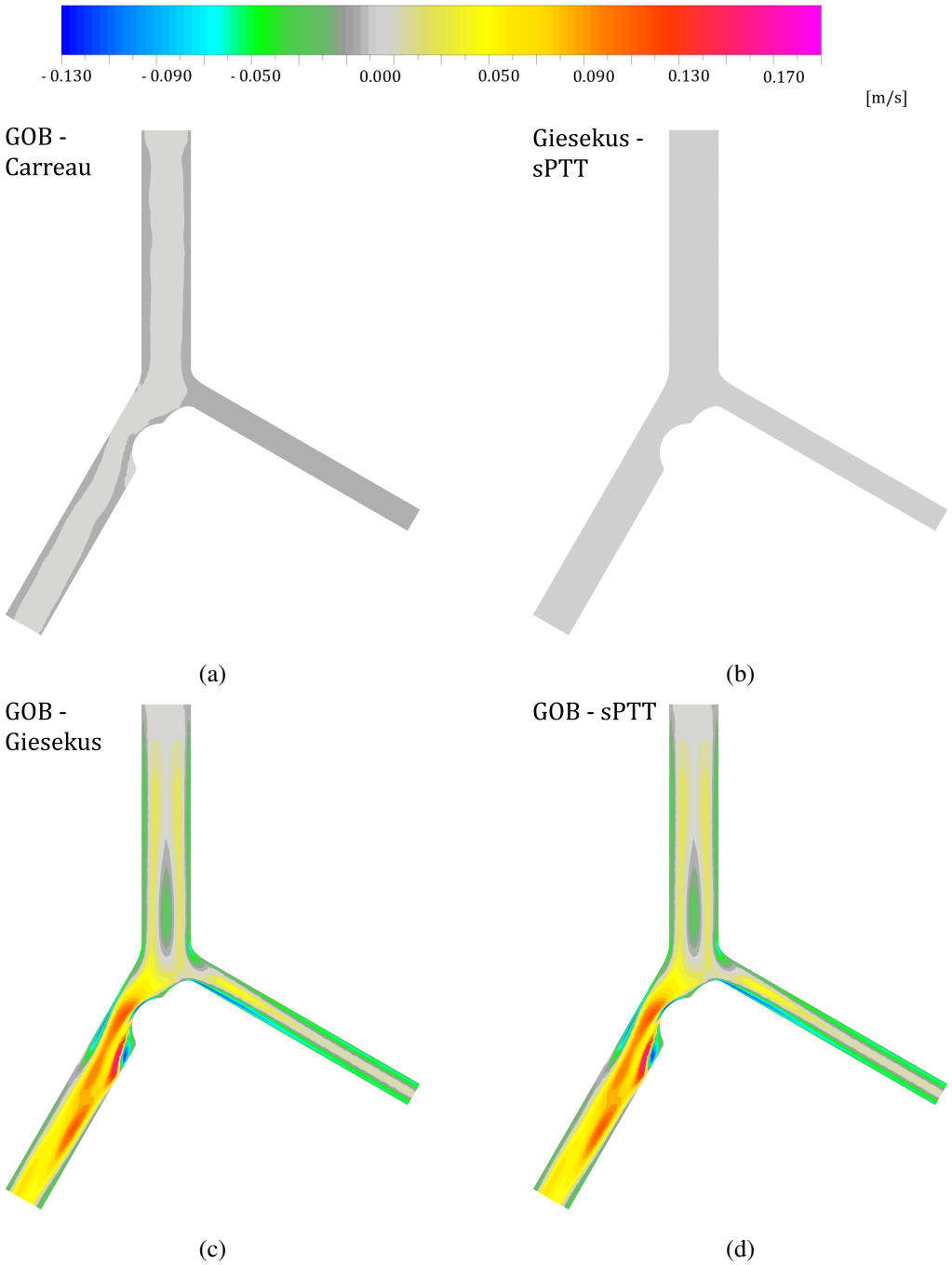

Figure 6.5: Axial velocity contours: difference between the non-Newtonian solutions for the idealized right coronary artery with a stenosed region after the bifurcation. (a) Difference between the GOB and the Carreau models. (b) Difference between the Giesekus and the sPTT models. (c) Difference between the GOB and the Giesekus models. (d) Difference between the GOB and the sPTT models.

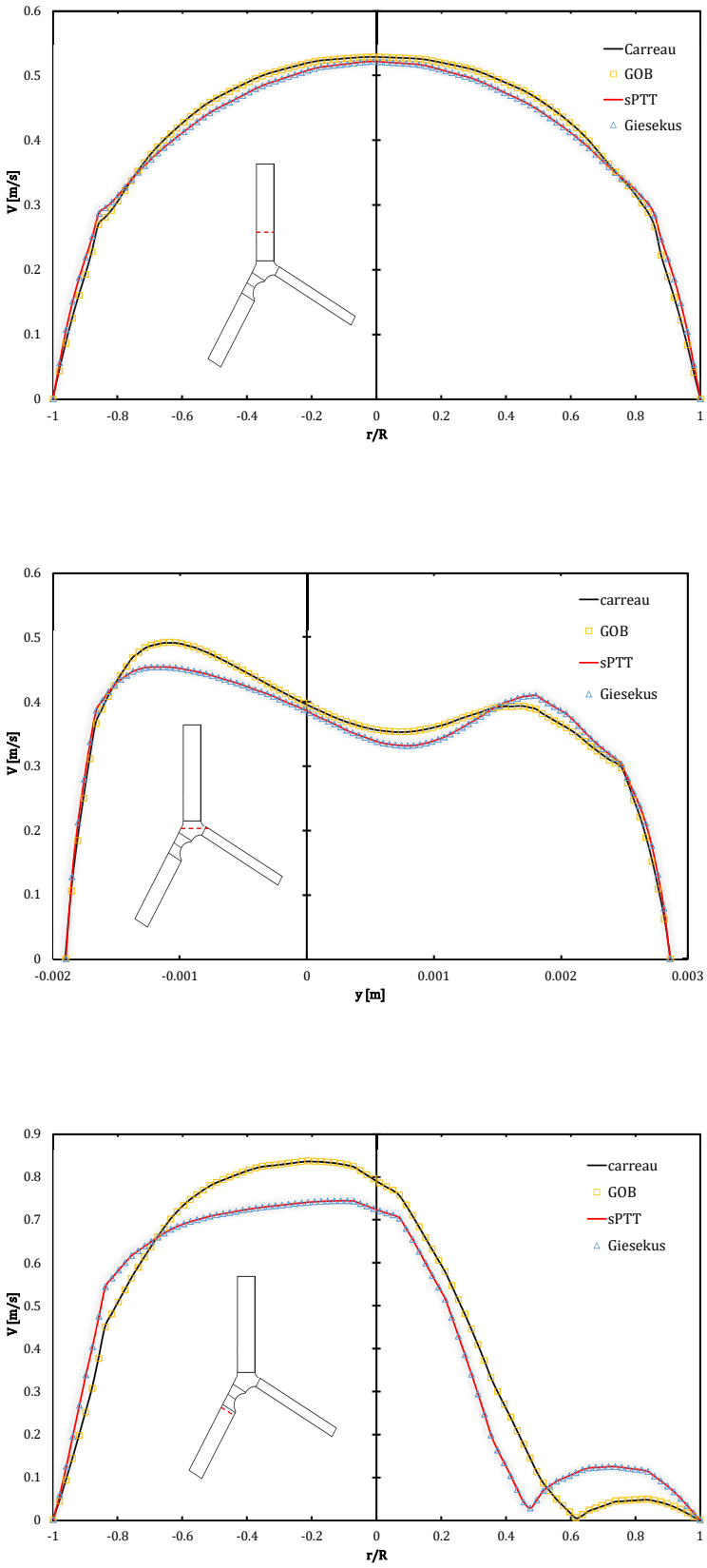

Figure 6.6: Velocity profiles along the mid plane of the artery for different non-Newtonian models. Red dashed lines in the schematics indicate the velocity profiles' position.

6.3 WSS

Although significant differences were found in the velocity fields when taking into account the viscoelasticity of blood, there was no large influence in the actual flow behaviour or streamline patterns. However, experimental evidence shows that elasticity has a remarkable effect upon the stress distribution [33]. While the main goal of this study is the implementation of more accurate rheological models for blood flow, if these are to be used to investigate the mechanics of atherosclerotic vessels, the effect of these models on WSS distribution is of great importance. As already mentioned a narrowing of the blood vessel will cause an increase in the wall shear stress and a rupture may occur. This decrease in the cross-section area of the vessels is known as atherosclerosis and it has been found that low WSS values lead to a haemodynamic behaviour more propitious to atherosclerotic plaque formation [3].

Figure 6.7 shows the WSS distribution for the different non-Newtonian solutions. Notice that the results seen in Figure 6.7 are now of the full 3D geometry, i.e., due to the definition of WSS itself the results are taken and must also be visualized at the surface walls. By analysing Figure 6.7, it is evident that there are significant differences in WSS magnitude for the multi-mode viscoelastic models and that once again there is no visible deviation of the implemented Generalized Oldroyd-B model when compared to the shear-thinning Carreau model. The Giesekus and sPTT solutions show an overall decrease in WSS. In particular, in the most critical region at the throat of the stenosis, these models predict peak WSS values close to half the magnitude (51%) of the Carreau model.

No previous works have been found for the same models or conditions. However, results seem to be in accordance to similar studies as the greatest differences in WSS are found at highly curved regions. These are the locations of peak WSS, similar for different models while varying only in magnitude [34]. Research has been done for other viscoelastic models that found lower WSS values for a pure Oldroyd-B model than for a shear-thinning Cross model (Section 4.3.1) [35], while in the present study the WSS values for the viscoelastic Giesekus and sPTT models were also lower than for the shear-thinning Carreau model.

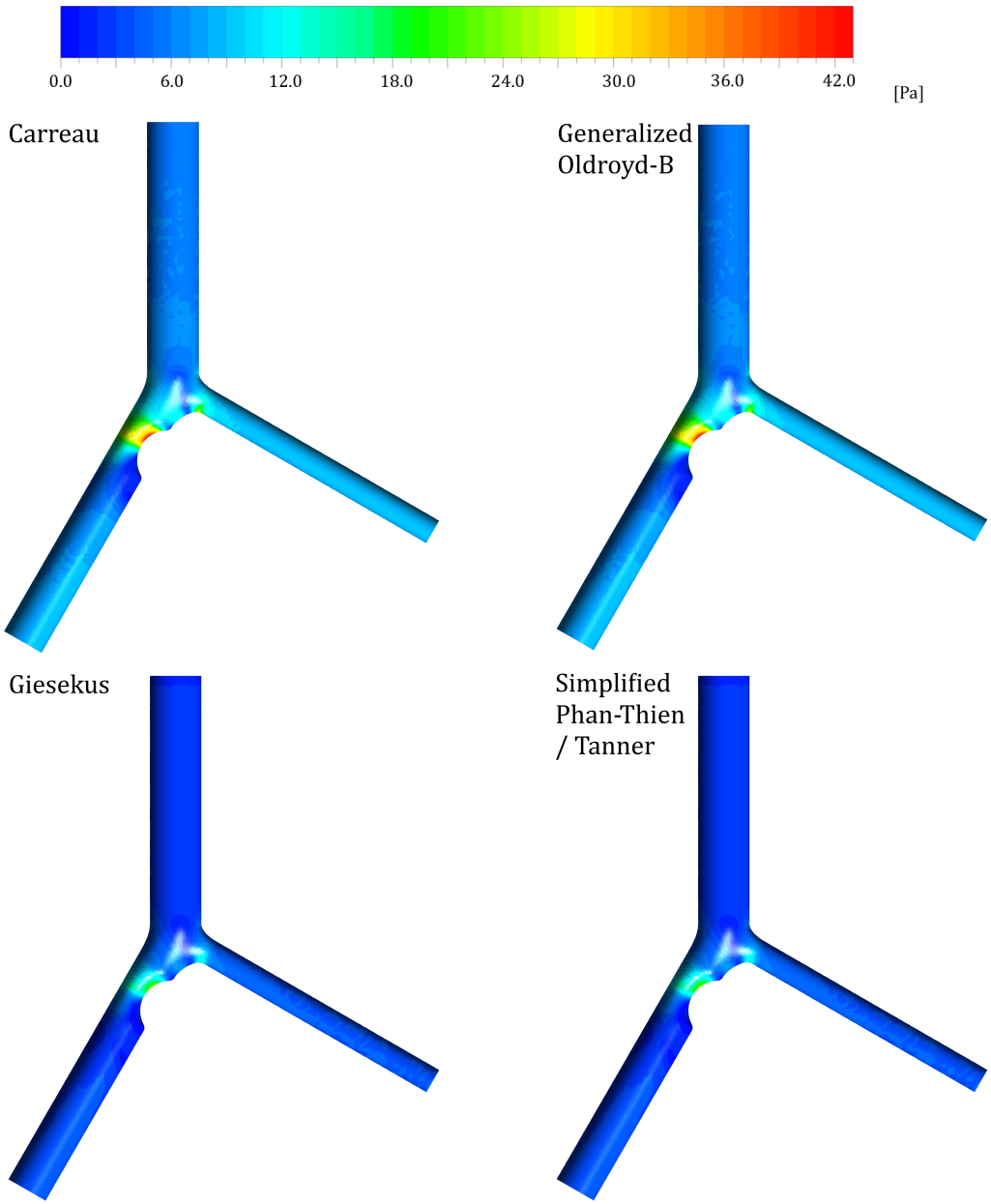

Figure 6.7: WSS magnitude in the idealized right coronary artery with a stenosed region after the bifurcation for the non-Newtonian solutions.

6.4 Application in patient-specific geometries

The haemodynamic descriptors introduced in Chapter 3 are of extreme importance in the detection of atherosusceptible regions. Therefore, their prediction must be as close as possible to reality. The main motivation of the present work was to understand the influence of the usage of more complex rheological models for blood, which additionally describe its viscoelastic behaviour, in the same WSS-based descriptors. In this section, the numeric procedure already described and applied to idealized blood vessels, was used in patient-specific right coronary artery (RCA) geometries. For idealized geometries the results from the simulations were plotted at a given time step, in this case the systolic peak. However, for patient-specific data the presented results of the WSS-based descriptors correspond to a time average along the cardiac cycle.

As already mentioned, the RCA has a very complex geometry. The tortuous nature of this artery can have a significant impact in haemodynamic behaviour. For this reason, there is a necessity to use more realist geometric models. Computed tomography (CT) scans of two healthy individuals, provided by the Department of Cardiology of the Gaia/Espinho Hospital Centre, were reconstructed into the three-dimensional models following the process described by Pinho et al. [3]. Blood flow was then simulated, allowing for the comparison of the generalized Newtonian Carreau model, used in previous works [30, 28, 3], and the newly introduced multi-mode simplified Phan-Thien/ Tanner (sPTT) viscoelastic model. To visualize the differences between the results by the using the two rheological models, the haemodynamic descriptors were calculated. The two geometries can be found in Figure 6.8, showing the expected increase in roughness and curvature as well as in the number of outlets, when compared to idealized vessels. The boundary conditions applied were once more adapted to the three-dimensional models in question by the Womersley number (Wo), with the values of 3.04 and 2.72, for Patient 1 and 2, respectively. These were calculated by considering the effective area of the inlet in each geometry and a consequent equivalent radius.

Figure 6.9 shows the distribution of the haemodynamic descriptor Time-Averaged Wall Shear Stress (TAWSS). Although usually associated with WSS magnitude and not directly with atherosclerotic plaque formation, regions with low WSS values are considered atherosusceptible [3]. In particular, regions with TAWSS values under 0.4 $[Pa]$ are critical in nature. Thus, in Figure 6.9 a reverse colour scale was used, where the warmer colours represent these same critical regions. For both patients, the sPTT model shows critical regions of increased size when compared to the Carreau model. This was expected due to the reduced WSS values previously found for the viscoelastic model (sPTT), in Section 6.3. A simple analysis of TAWSS values under 0.4 $[Pa]$, in terms of superficial area, shows that when using the Carreau model no percentage of the total area actually reaches values lower than 0.4 $[Pa]$. While for the sPTT model, regions susceptible to plaque formation can be seen, representing 0.20% and 0.72% of the total area in Patient 1 and Patient 2, respectively. Although the percentage of critical area is low, meaning that both patients have a reduced tendency for atherosclerosis development, the differences between the models are notable.

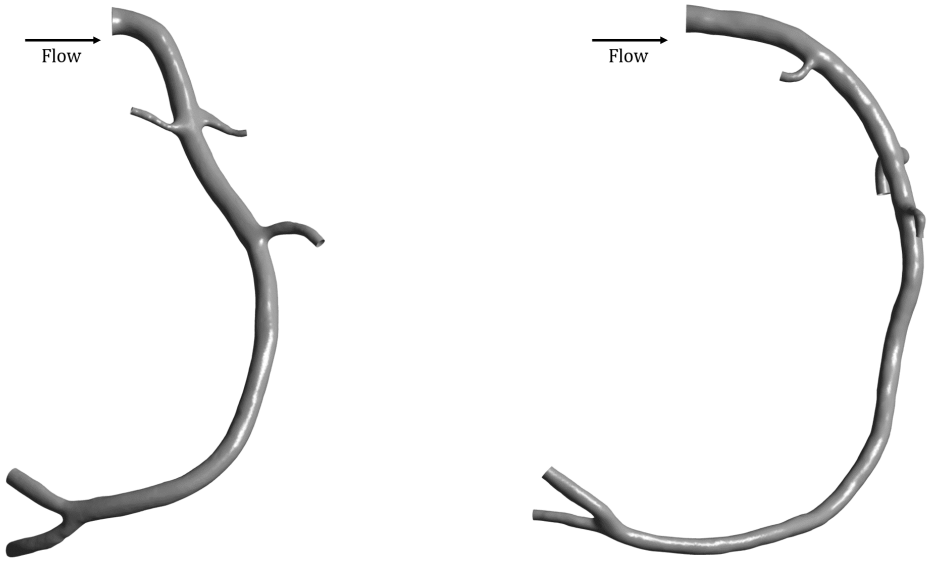

Figure 6.8: Reconstructed right coronary arteries: (a) Patient 1 and (b) Patient 2.

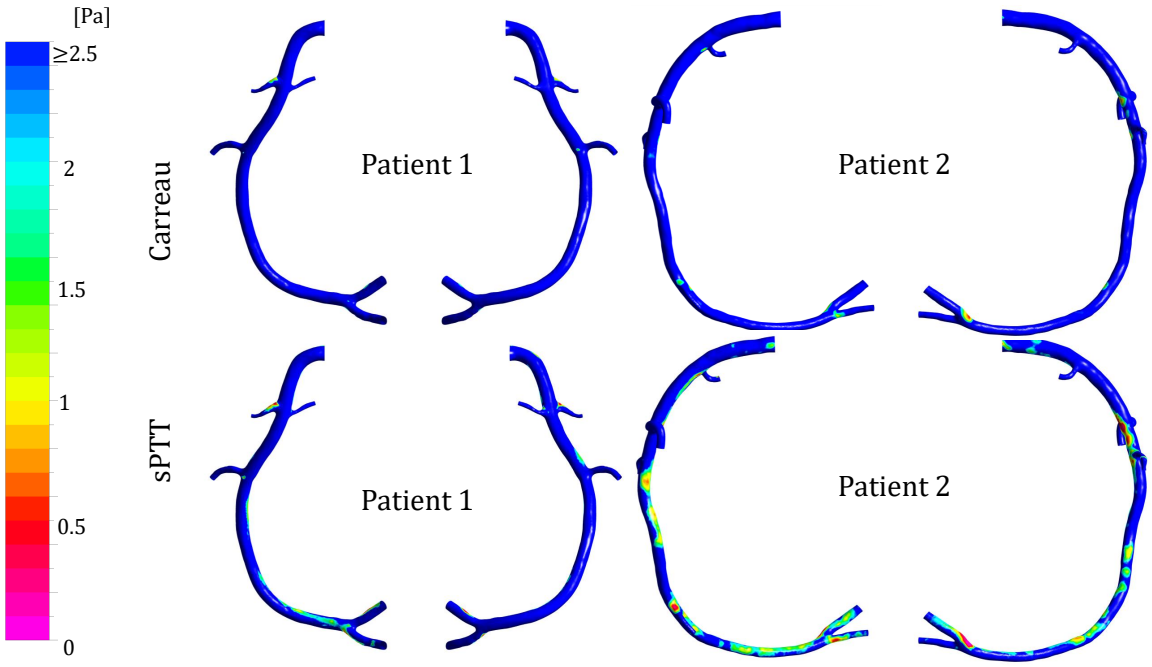

Figure 6.9: TAWSS distribution in the studied RCA cases using two different rheological models for blood.

The Oscillatory Shear Index (OSI) distribution is shown in Figure 6.10. While it is possible to see differences between the Carreau and sPTT models, these are not significant. Even considering the increase of OSI values in certain regions near the bifurcations when the viscoelastic model is used, low OSI values are common in healthy right coronary arteries. Despite showing increased

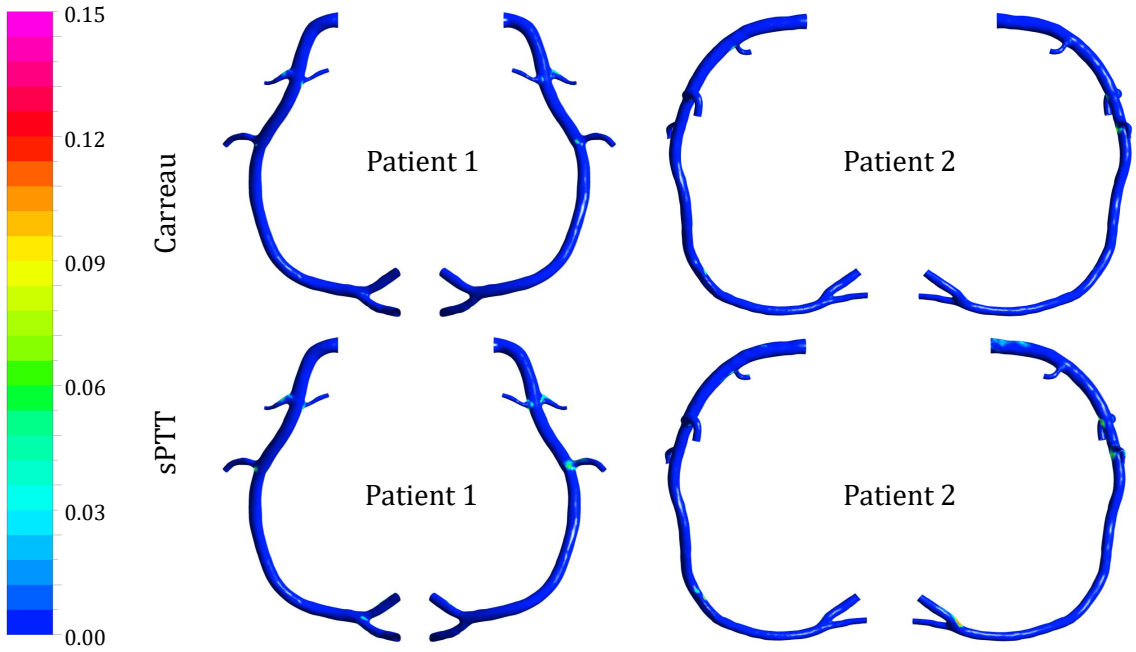

Figure 6.10: OSI distribution in the studied RCA cases using two different rheological models for blood.

curvature when compared to idealized geometries, the modelled patient-specific arteries can still be considered to have low tortuosity when compared to most cases. Higher values for this haemodynamic descriptor are usually found in stenosed arteries, due to the higher flow disturbance, but by itself OSI is usually considered the less relevant of the WSS-based descriptors [3].

RRT appears as the most robust metric for the assessment of regions prone to the appearance of atherosclerosis, showing the lowest number of false positives, since it is directly dependent on OSI and inversely dependent on TAWSS [3]. Figure 6.11 shows the Relative Residence Time (RRT) distribution in both patients. Once again, it is possible to observe a clear increase in the haemodynamic descriptor values for the viscoelastic sPTT model. When considering the viscoelastic model in Patient 2, it is even possible to identify a critical region (RRT$>$ 8 $[Pa^{-1}]$) near the outer wall of the final bifurcation. As mentioned in Section 2.3, this is a common behaviour, as atherosclerosis is usually found in high curvature zones and in the outer walls of bifurcations.

Another important point to take note of is the computational time. Due to the choice of a non-linear multi-mode rheological model, one that is being added as an extra set of equations, there will be a relevant increase in the computational time. This increase in has an increased significance when considering larger computational domains, such as patient-specific right coronary arteries. The simulations of the present section were performed in computer with 32 GB of RAM, powered by an *Intel® Core™ i7-7700K Processor* with 8M Cache and a base frequency of 4.20GHz. Regarding the Carreau model the simulations had an average time, for both patients, of 1.5 *hours*, while when using the multi-mode viscoelastic sPTT model the computational time reached an average of 8 *hours*.

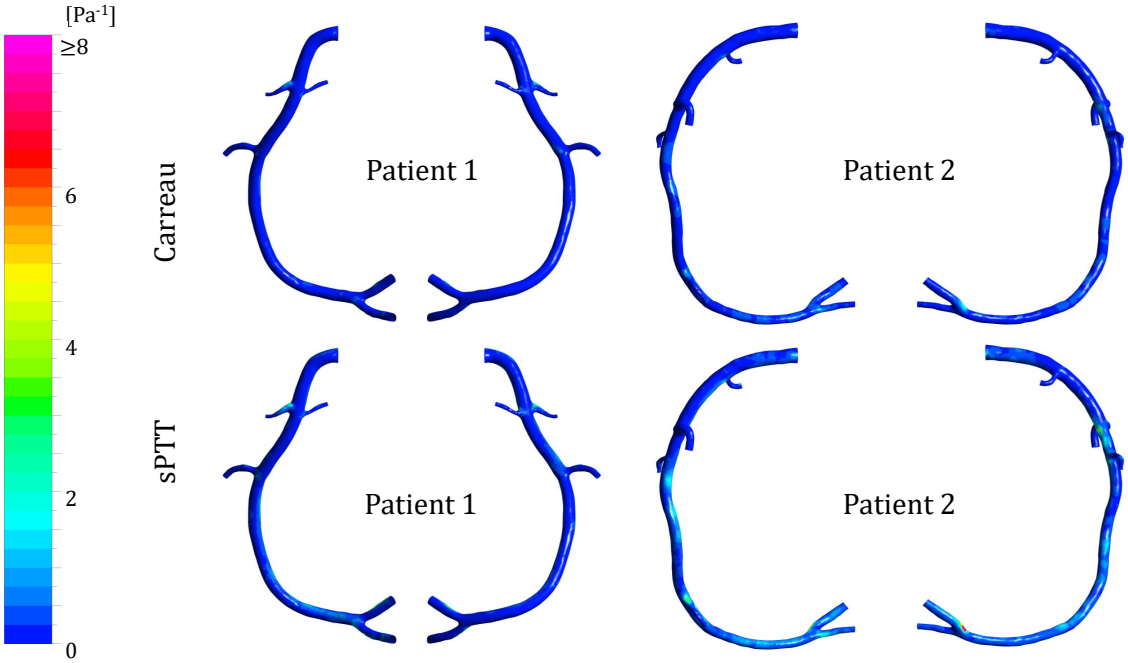

Figure 6.11: RRT distribution in the studied RCA cases using two different rheological models for blood.

Chapter 7

Conclusions

This thesis focuses on the numerical study of blood flow while considering the non-Newtonian characteristic of blood, viscoelasticity. Three viscoelastic constitutive models for blood where implemented in the commercial CFD solver ANSYS Fluent. The desired elastic effects were modelled as additional source terms of the governing equations, through the use of User-Defined Functions, a way to enhance the solver's capabilities.

It has been found that through the described means, ANSYS Fluent is capable of modelling viscoelastic behaviour and is a viable option against other in-house solvers. After the code development, the performed simulations were of simple use due to the miscellaneous commodities and the user-friendly layout of the commercial software package Workbench ANSYS.

In regard to the results obtained, the more popular constitutive models for blood, widely used by many authors, such as the Newtonian solution and the previously used Carreau shear-thinning model, were directly compared, in terms of flow behaviour, to those using considering the viscoelastic (shear-thinning and elastic) properties of blood. In a first stage, the simulations performed in idealized geometries found that the shear-thinning effects of the solvent contribution of the Generalized Oldroyd-B model are more pronounced than the viscoelastic ones. This effect can be seen in the comparison between the solutions for this model and the Carreau model. This outcome is coherent with similar studies, although not as clear as in the present work, where the solutions for the models of different nature where found to be almost equivalent. As expected, the viscoelastic effects were more pronounced for the multi-mode viscoelastic constitutive models, Giesekus and Simplified Phan-Thien/ Tanner. These models show a general reduction in velocity, a behaviour that becomes sharper in zones of higher velocity gradients, such as the bifurcations and the stenosis, as well as smaller recirculation zones. It should also be noted that the results for the different rheological models where found coherent for the distinct idealized right coronary arteries. As both the Giesekus and sPTT multi-mode models have shown identical results, the sPTT model has been found the better option for the modelling of the viscoelastic behaviour of blood, due to its more accurate depiction of the physical properties of blood. The differences between the viscoelastic constitutive models and the more commonly used Newtonian and Generalized Newtonian models where found significant. The reduction in velocity seen in the multi-mode models

results in a decrease of the wall shear stress distribution, the difference in peak WSS values being close to half the magnitude (51%) of the Carreau model.

In a second stage, using patient-specific geometries of right coronary arteries, the influence of the chosen viscoelastic rheological model in the haemodynamic descriptors, used in the prevention and diagnosis of atherosclerotic disease, was studied. In both of the two reconstructed right coronary arteries, the WSS reduction throughout the cardiac cycle resulted in an expected drop in the values of the Time Averaged Wall Shear Stress parameter. The impact of a viscoelastic constitutive model for blood, the sPTT multi-mode model, on the WSS-based descriptors allows for the conclusion that this choice of rheological model is indeed justifiable. In fact, and depending on the geometry, the conclusion of the diagnostic can even change due to the appearance of new critical regions (atherosusceptible zones), according to the criteria of the haemodynamic descriptors. As such, in order to obtain a more reliable and realistic tool for the prevention and diagnosis of atherosclerotic disease, the viscoelastic properties of blood should be considered, especially in smaller arteries and vessels with complex geometries.

7.1 Future works

Despite the extensive work and the interesting results obtained throughout this thesis, some recommendations for further development should be made.

As already mentioned, no previous works for the numerical simulation of unsteady pulsatile blood flow, with time-varying pressure profile imposed at the outlets and with a choice of viscoelastic rheological models for blood were found. Thus, other simulations, through different already validated solvers, could be performed under the same current models, conditions and geometries, in order to compare such results with those obtained in this thesis after the implementation of the viscoelastic properties.

The developed UDF based code that was implemented in ANSYS Fluent could also be optimized in order to account for parallel computing capabilities. This would result in a considerable reduction of the computational time of the simulations.

The rheological model for blood should be as accurate as possible. To move a step further on this topic, more complex models for blood flow could be used. Ideally, in addition to viscoelastic properties of blood, these models should also reflect the specific mechanisms that affect those rheological properties. For example, the model developed by Anand and Rajagopal [36] falls under this category. This model has a thermodynamic framework leading a characterization of blood's elasticity, the viscosity of plasma, the formation of rouleaux and their effect on the viscosity of blood, along with it's shear-thinning behaviour [36].

Finally, for a more realistic assessment of the blood flow dynamics through the use of numerical simulations, while following a patient-specific approach, the current methodology could be upgraded by considering realistic arterial wall deformation models that are able to reflect its mechanical behaviour. This fluid-structure interaction (FSI) analysis can also be done resorting

to tools included in Workbench ANSYS. Tests considering both FSI and the viscoelastic properties of blood should be done and compared to those which assume rigid walls. The conclusions for this comparison would have a special significance as depending on whether FSI (deformable walls) is found to make a relevant difference on the results or not, there will be a large impact on the computational time of the simulations.

References

[1] Marc Thiriet e Kim H. Parker. *Physiology and pathology of the cardiovascular system: A physical perspective*, páginas 1–45. Springer Milan, 2009.

[2] G.J. Tortora e B.H. Derrickson. *Principles of Anatomy and Physiology*. Wiley, 2015.

[3] N. Pinho, L. C. Sousa, C. F. Castro, C. C. António, M. Carvalho, W. Ferreira, R. Ladeiras-Lopes, N. D. Ferreira, P. Braga, N. Bettencourt, e S. I. S. Pinto. The impact of the right coronary artery geometric parameters on hemodynamic performance. *Cardiovascular Engineering and Technology*, 2019.

[4] Nelson Pinho, Marco Bento, Luisa Sousa, S.I.s Pinto, Catarina Castro, Carlos Conceição António, e Elsa Azevedo. Patient-specific study of a stenosed carotid artery bifurcation using fluid–structure interactive simulation. volume 27, páginas 495–503, 2018.

[5] Fuat Yilmaz e Mehmet Yaar Gundogdu. A critical review on blood flow in large arteries; relevance to blood rheology, viscosity models, and physiologic conditions. *KOREA-AUSTRALIA RHEOLOGY JOURNAL*, 20(4):197–211, 2008.

[6] Laura Campo-Deaño, Mónica Oliveira, e Fernando T. Pinho. A review of computational hemodynamics in middle cerebral aneurysms and rheological models for blood flow. *Applied Mechanics Reviews*, 67:030801, 2015.

[7] S. Standring. *Gray's Anatomy: The Anatomical Basis of Clinical Practice*. Gray's Anatomy. Elsevier Health Sciences, 2015.

[8] O.K. Baskurt, M.R. Hardeman, e M.W. Rampling. *Handbook of Hemorheology and Hemodynamics*. Biomedical and health research. IOS Press, 2007.

[9] B.R. Munson, A.P. Rothmayer, e T.H. Okiishi. *Fundamentals of Fluid Mechanics, 7th Edition*. Wiley, 2012.

[10] J.L. Poiseuille. *Recherches expérimentales sur le mouvement des liquides dans les tubes de très-petits diamêtres*. Imprimerie Royale, 1844.

[11] F.A. Morrison. *Understanding Rheology*. Raymond F. Boyer Library Collection. Oxford University Press, 2001.

[12] N. Phan-Thien. *Understanding Viscoelasticity: An Introduction to Rheology*. Graduate Texts in Physics. Springer Berlin Heidelberg, 2012.

[13] Denis Doorly e Spencer Sherwin. *Geometry and flow*, páginas 177–209. Springer Milan, 2009.

[14] Demosthenes Katritsis, Lambros Kaiktsis, Andreas Chaniotis, John Pantos, Efstathios P. Efstathopoulos, e Vasilios Marmarelis. Wall shear stress: Theoretical considerations and methods of measurement. *PROGRESS IN CARDIOVASCULAR DISEASES*, 49(5):307–329, 2007.

[15] Amirhossein Arzani e Shawn C. Shadden. Characterizations and Correlations of Wall Shear Stress in Aneurysmal Flow. *JOURNAL OF BIOMECHANICAL ENGINEERING-TRANSACTIONS OF THE ASME*, 138(1), 2016.

[16] Sang-Wook Lee, Luca Antiga, e David A. Steinman. Correlations Among Indicators of Disturbed Flow at the Normal Carotid Bifurcation. *JOURNAL OF BIOMECHANICAL ENGINEERING-TRANSACTIONS OF THE ASME*, 131(6), 2009. ASME Summer Bioengineering Conference, Marco Isl, FL, JUN 25-29, 2008.

[17] A.P. Deshpande, J.M. Krishnan, e S. Kumar. *Rheology of Complex Fluids*. Rheology of Complex Fluids. Springer New York, 2010.

[18] OK Baskurt e HJ Meiselman. Blood rheology and hemodynamics. *SEMINARS IN THROMBOSIS AND HEMOSTASIS*, 29(5):435–450, 2003.

[19] N. Bessonov, A. Sequeira, S. Simakov, Yu. Vassilevskii, e V. Volpert. Methods of Blood Flow Modelling. *MATHEMATICAL MODELLING OF NATURAL PHENOMENA*, 11(1):1–25, 2016.

[20] Andreja Zupančič Valant, Lovro Žiberna, Yannis Papaharilaou, Andreas Anayiotos, e Georgios C. Georgiou. The influence of temperature on rheological properties of blood mixtures with different volume expanders—implications in numerical arterial hemodynamics simulations. *Rheologica Acta*, 50(4):389–402, 2011.

[21] George B Thurston. Viscoelastic properties of blood and blood analogs. *Advances in hemodynamics and hemorheology*, 1:1–30, 1996.

[22] PCF Moller, J Mewis, e D Bonn. Yield stress and thixotropy: on the difficulty of measuring yield stresses in practice. *SOFT MATTER*, 2(4):274–283, 2006.

[23] R.G. Larson e H. Brenner. *Constitutive Equations for Polymer Melts and Solutions: Butterworths Series in Chemical Engineering*. Butterworths series in Chemical Engineering. Elsevier Science, 2013.

[24] R.B. Bird e O. Hassager. *Dynamics of Polymeric Liquids: Fluid mechanics*. Dynamics of Polymeric Liquids. Wiley, 1987.

[25] A. Farina, A. Mikelić, L. Fusi, F. Rosso, G. Saccomandi, A. Sequeira, e E.F. Toro. *Non-Newtonian Fluid Mechanics and Complex Flows: Levico Terme, Italy 2016*. Lecture Notes in Mathematics. Springer International Publishing, 2018.

[26] Young Cho e Kenneth R. Kensey. Effects of the non-newtonian viscosity of blood on flows in a diseased arterial vessel. part 1: Steady flows. *Biorheology*, 28:241–62, 1991.

[27] Laura Campo-Deano, Roel P. A. Dullens, Dirk G. A. L. Aarts, Fernando T. Pinho, e Monica S. N. Oliveira. Viscoelasticity of blood and viscoelastic blood analogues for use in polydymethylsiloxane in vitro models of the circulatory system. *BIOMICROFLUIDICS*, 7(3), 2013.

[28] N. Pinho, C. F. Castro, C. C. António, N. Bettencourt, L. C. Sousa, e S. I. S. Pinto. Correlation between geometric parameters of the left coronary artery and hemodynamic descriptors of atherosclerosis: Fsi and statistical study. *Medical & Biological Engineering & Computing*, 57(3):715–729, 2019.

[29] T. Bodnár, A. Sequeira, e M. Prosi. On the shear-thinning and viscoelastic effects of blood flow under various flow rates. *Applied Mathematics and Computation*, 217(11):5055 – 5067, 2011. Numerical Analysis of Fluid Flow and Heat Transfer.

[30] N. Pinho, L. C. Sousa, C. F. Castro, C. C. António, M. Carvalho, W. Ferreira, R. Ladeiras-Lopes, N. D. Ferreira, P. Braga, N. Bettencourt, e S. I. S. Pinto. The impact of the right coronary artery geometric parameters on hemodynamic performance. *Cardiovascular Engineering and Technology*, 2019.

[31] S. A. Berger e L-D. Jou. Flows in stenotic vessels. *Annual Review of Fluid Mechanics*, 32(1):347–382, 2000.

[32] R. Rannacher e A. Sequeira. *Numerical Study of the Significance of the Non-Newtonian Nature of Blood in Steady Flow Through a Stenosed Vessel*. Springer Berlin Heidelberg, 2010.

[33] C. Balan, V. Legat, A. Neagoe, e D. Nistoran. Experimental investigations and numerical simulations for an open channel flow of a weak elastic polymer solution around a t-profile. *Experiments in Fluids*, 36(3):408–418, 2004.

[34] Bryan C. Good, Steven Deutsch, e Keefe B. Manning. Hemodynamics in a pediatric ascending aorta using a viscoelastic pediatric blood model. *Annals of Biomedical Engineering*, 44(4):1019–1035, 2016.

[35] A. Javadzadegan, M. Esmaeili, S. Majidi, e B. Fakhimghanbarzadeh. Pulsatile flow of viscous and viscoelastic fluids in constricted tubes. *Journal of Mechanical Science and Technology*, 23(9):2456–2467, 2009.

[36] M Anand e Kr Rajagopal. A shear-thinning viscoelastic blood model for describing the flow of blood. *Int. J. Cardiovascular Medicine and Science*, 4, 2004.

Appendix A

Direct flow differences: remaining geometries

In this Appendix results complementary to Section 6.2 regarding the direct flow differences between the rheological models are presented.

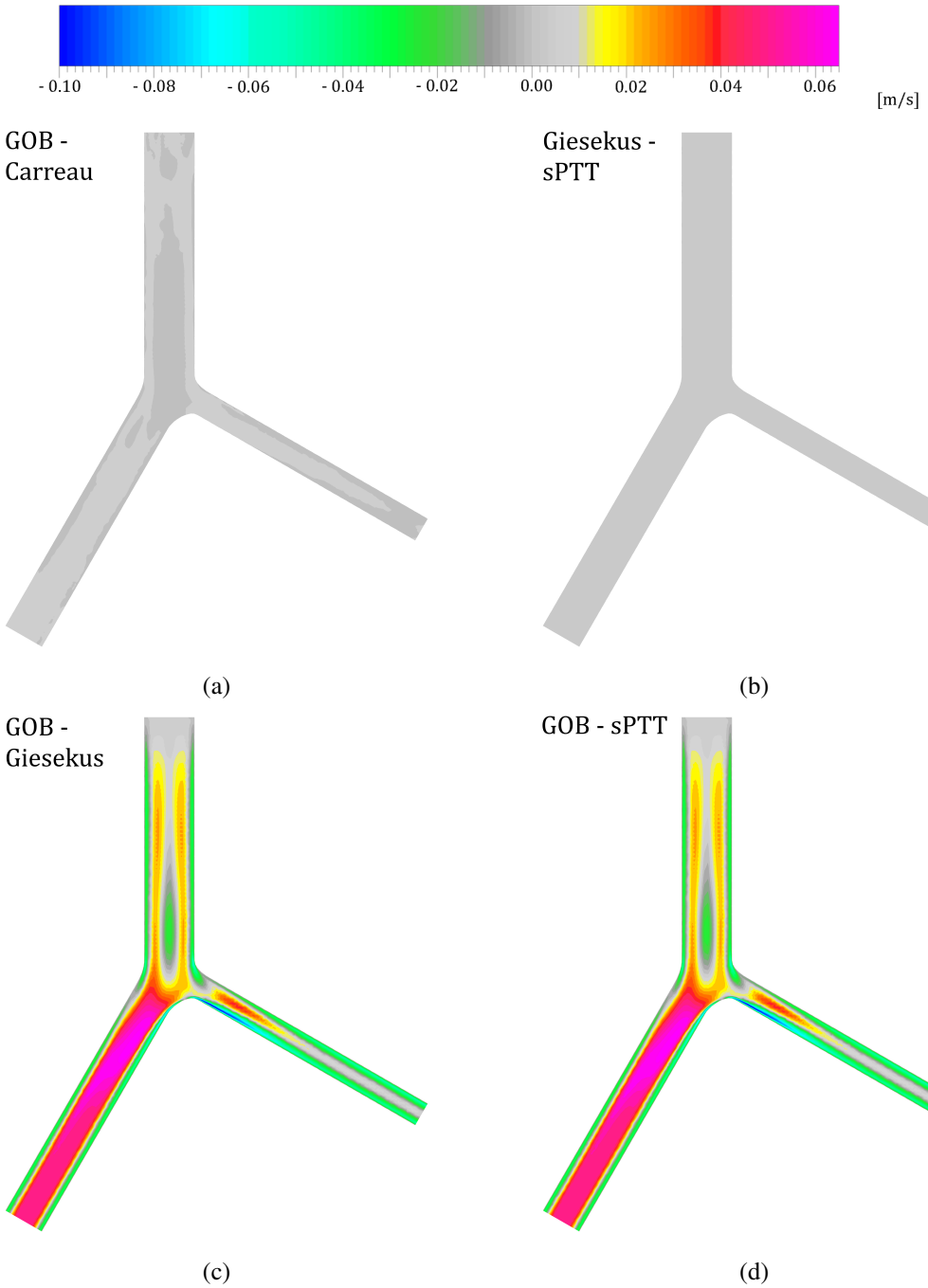

Figure A.1: Axial velocity contours: difference between the non-Newtonian solutions for the idealized healthy right coronary artery. (a) Difference between the GOB and the Carreau models. (b) Difference between the Giesekus and the sPTT models. (c) Difference between the GOB and the Giesekus models. (d) Difference between the GOB and the sPTT models.

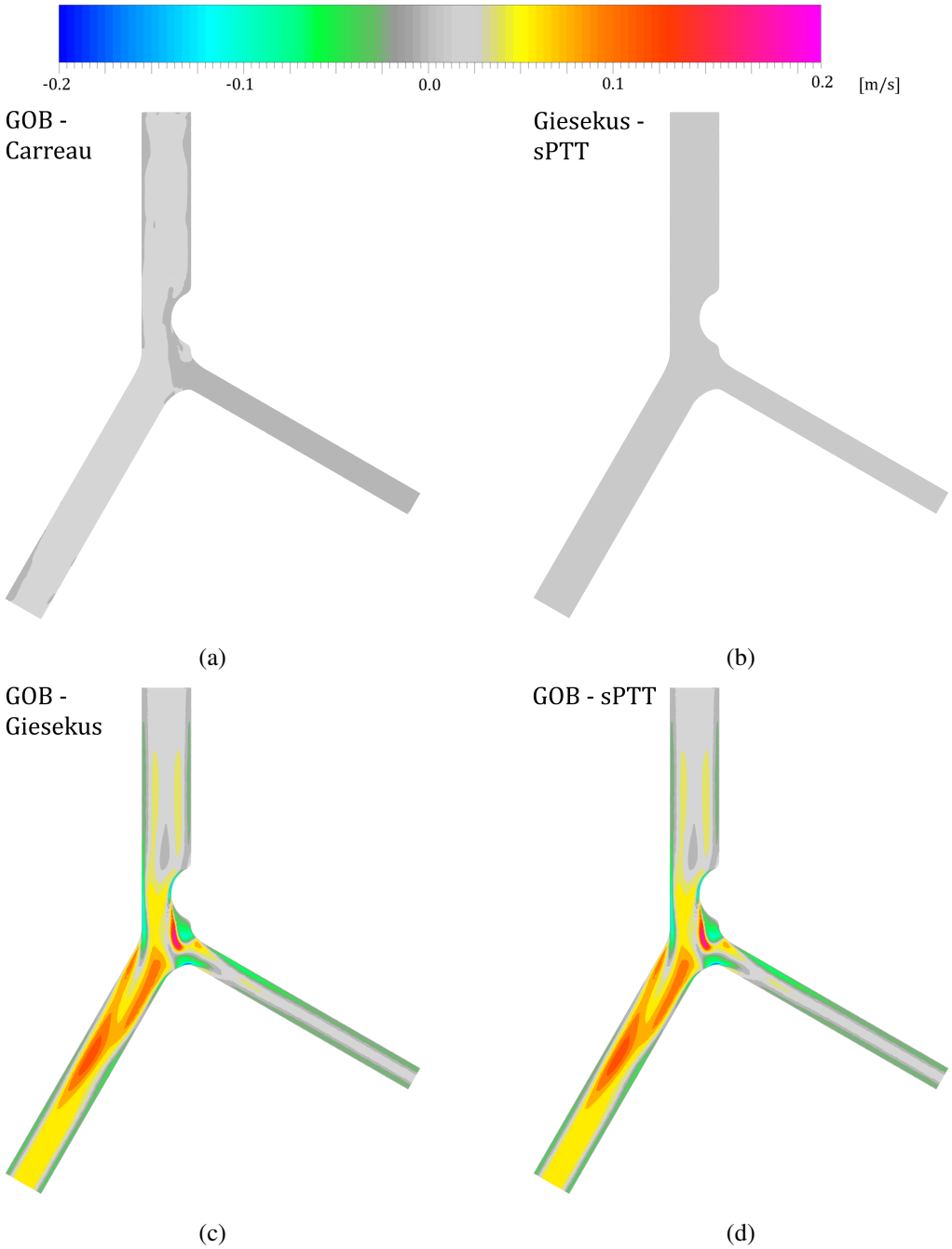

Figure A.2: Axial velocity contours: difference between the non-Newtonian solutions for the idealized right coronary artery with a stenosed region before the bifurcation. (a) Difference between the GOB and the Carreau models. (b) Difference between the Giesekus and the sPTT models. (c) Difference between the GOB and the Giesekus models. (d) Difference between the GOB and the sPTT models.

Appendix B

Abstracts of articles presented at an international conference

The following abstracts were accepted and presented in the *ICoNSoM 2019 - International Conference of Nonlinear Solid Mechanics, 16-19 June, Roma, Italy* and are based on the works of this dissertation.

I prefer: ORAL presentation

NONLINEAR VISCOELASTIC PROPERTY OF BLOOD FOR HEMODYNAMIC SIMULATIONS – CODE DEVELOPMENT

E. Romano, L.C. Sousa, C.C. António, C.F. Castro, S.I.S. Pinto

FEUP, LAETA-INEGI, Porto, Portugal

spinto@fe.up.pt

Hemodynamic simulations have proven to be an auxiliary clinical tool with great potential for diagnosis and the development of preventive measures and treatments of cardiovascular diseases. Therefore, simulations with complex rheology of blood are of great interest since the most accurate hemodynamic is essential for clinical practice. Several authors have used a large range of models defining the rheological behavior of blood, ranging from the most common Newtonian and Generalized Newtonian models to non-Newtonian viscoelastic models. The viscoelastic character of blood is due to the storage and release of elastic energy from RBC aggregates. There is a need in the use of models depicting this behavior.

The aim of this study is to take a step forward in the numerical simulation of blood flow through the implementation and validation of a more accurate rheological model for blood in *User-Defined Functions* (UDF) associated to the basis of *Ansys*® software. 3D idealized geometries of a stenosed bifurcation in a right coronary artery were used along with time-dependent velocity and pressure profiles of pulsatile flow and pressure waveforms as boundary conditions. Two different nonlinear viscoelastic non-Newtonian models able to predict shear-thinning behavior - a Generalized Oldroyd-B model and a multi-mode Giesekus model - were compared with a simpler Generalized Newtonian model – Carreau Model. The effect of the viscoelastic components of stress can be seen through the axial velocity contours in Fig. 1. The biggest impact is generated in the regions with high velocity gradients and significant differences were observed when considering Giesekus model relative to Oldroyd-B or Carreau model.

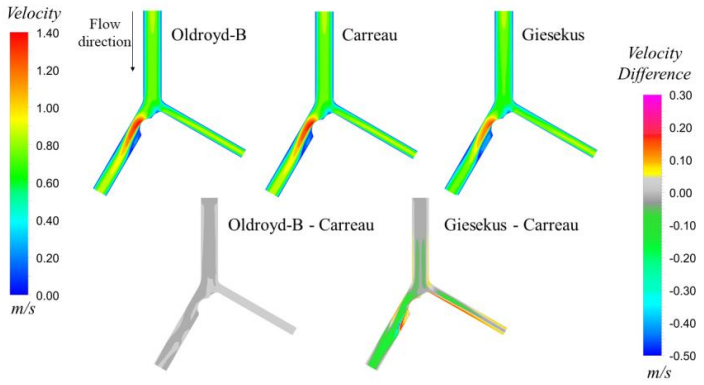

Fig. 1: Velocity contours along the middle plane of the 3D geometry for the different rheological models (top) and velocity difference between the Viscoelastic and the Generalized Newtonian (Carreau) models (bottom).

I prefer: POSTER presentation

WSS DESCRIPTORS IN A PATIENT RCA CONSIDERING NONLINEAR VISCOELASTICITY OF BLOOD

E. Romano, L.C. Sousa, C.C. António, C.F. Castro, S.I.S. Pinto

FEUP, LAETA-INEGI, Porto, Portugal

spinto@fe.up.pt

Cardiovascular diseases, such as atherosclerosis development in arteries, are one of the most common causes of death in developed countries. The study of blood flow in patient-specific cases became highly relevant in clinical practice due to a need for understanding the mechanical stresses induced on the vessels. Hemodynamic simulations using computed tomography (CT) image-based geometries of blood vessels, with all the conditions as close as possible to the patient, has been a powerful auxiliary tool for prevention, diagnosis and treatment of atherosclerosis disease. Therefore, authors intend to model, for simulations, the most accurate behavior of blood. The rheological behavior of blood in the heart and large blood vessels is usually characterized as Newtonian. However, it is well-known that blood is a viscoelastic non-Newtonian fluid and should be modeled as such, especially when considering the pulsatile nature of blood flow and arteries of smaller size.

The present work is focused on numerical studies of blood flow in patient-specific right coronary arteries (RCA), using *Ansys*® software. The hemodynamic behavior under two different rheological models for blood - the Carreau model, a Generalized Newtonian Model (GNM), and the multi-mode Giesekus model, a nonlinear viscoelastic non-Newtonian model - were compared. These models were already implemented and validated in *Ansys*® through 3D idealized geometries. Moreover, pulsatile flow was considered and the time-dependent velocity and pressure profiles as boundary conditions. Fig. 1 shows the relative residence time (RRT) spatial distribution, the strongest metric for assessing atherosclerotic formation. This hemodynamic descriptor indicates the particles' residence time near the arterial wall. Values greater than 8 Pa^{-1} are considered elevated showing atherosusceptible regions. Using the viscoelastic model or the GNM, the critical regions are in similar specific locations. However, when the viscoelastic model is considered, these critical regions are larger, meaning a higher tendency for atherosclerosis appearance and the importance of the viscoelastic model's use.

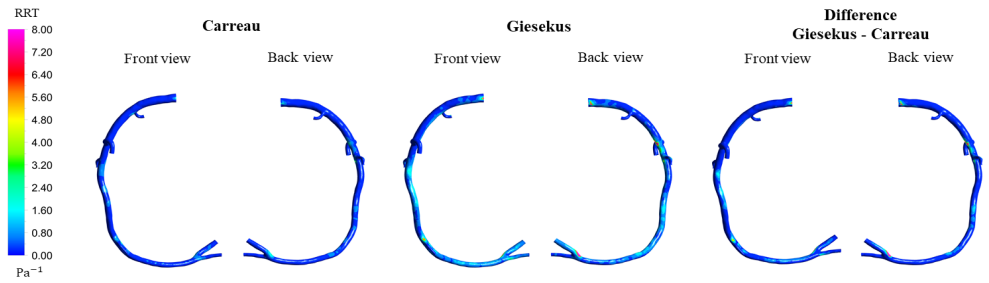

Fig. 1: RRT considering GNM (Carreau) and viscoelastic model (Giesekus); and difference between the models.